

Magnetosheath - Cusp Interface.

S. SAVIN¹, L. ZELENYI¹, S. ROMANOV¹, I. SANDAHL², J. PICKETT¹³, E. AMATA⁶, L. AVANOV¹,
 J. BLECKI⁹, E. BUDNIK¹, J. BUECHNER¹⁰, C. CATTELL¹⁵, G. CONSOLINI⁶, J. FEDDER¹¹, S. FUSELIER⁷,
 H. KAWANO⁴, S. KLIMOV¹, V. KOREPANOV¹⁶, D. LAGOUTTE¹², F. MARCUCCI⁶, M. MOGILEVSKY¹,
 Z. NEMECEK⁸, B. NIKUTOWSKI¹⁰, M. NOZDRACHEV¹, M. PARROT¹², J.L. RAUCH¹², V. ROMANOV¹,
 T. ROMANTSOVA¹, C. T. RUSSELL⁵, J. SAFRANKOVA⁸, J. A. SAUVAUD¹⁴, A. SKALSKY¹,
 V. SMIRNOV¹, K. STASIEWICZ^{3,9}, J.G. TROTIGNON¹², YU. YERMOLAEV¹

¹ *Space Research Institute, Russian Academy of Sciences, Profsoyuznaya 84/32, Moscow, 117810, Russia*

² *Swedish Inst. Space Physics, Kiruna, Sweden*

³ *Swedish Inst. Space Physics, Uppsala, Sweden*

⁴ *Kyushu U., Japan*

⁵ *IGPP, UCLA, USA*

⁶ *Interplanetary Space Phys. Inst., CNR, Roma, Italy*

⁷ *Lockheed Martin Alto Res. Lab., CA, USA*

⁸ *Faculty Math. Phys., Charles U., Praha, Czech Republic*

⁹ *Space Res. Center, Polish Academy Sci., Warsaw, Poland*

¹⁰ *Max-Planck Inst. Aeronomie, Katlenburg-Lindau, Germany*

¹¹ *Naval Research Lab., Washington, USA*

¹² *Laboratory Phys. Chemistry Environment, Orleans, France*

¹³ *U. Iowa, USA*

¹⁴ *Centre d'Etude Spatiale des Rayonnements, Toulouse, France*

¹⁵ *U. Minnesota, USA*

¹⁶ *Lviv Center for Space Researches, Ukraine*

ssavin@iki.rssi.ru, Fax: (7) 095 310 7023, Phone (7) 095 333 1100

The paper devoted to the INTERBALL Project results

1 ABSTRACT

We advance the achievements of Interball-1 and other contemporary missions in exploration of the magnetosheath-cusp interface. Extensive discussion of published results is accompanied by presentation of new data from a case study and a consideration of those data within the broader context of one-year Interball-1 statistics. Multi-spacecraft boundary layer studies reveal that in ~83 % of the cases the interaction of the magnetosheath (MSH) flow with the high latitude magnetopause produces a layer containing strong nonlinear turbulence, called the turbulent boundary layer (TBL). The TBL contains wave trains with flows at approximately the Alfvén speed along field lines and ‘diamagnetic bubbles’ with small magnetic fields inside. A comparison of the multi-point measurements obtained on May 29, 1996 with a global MHD model indicates that three types of populating processes should be operative:

- large-scale (~ few Re) antiparallel merging at sites remote from the cusp;
- medium-scale (few thousand km) local TBL-merging of fields that are antiparallel on average;
- small-scale (few hundred km) bursty reconnection of fluctuating magnetic fields, representing a continuous mechanism for MSH plasma inflow into the magnetosphere, which could dominate in quasi-steady cases.

The lowest frequency (~ 1-2 mHz) TBL fluctuations are traced throughout the magnetosheath from the post-bow shock region up to the inner magnetopause border. The resonance of these fluctuations with dayside flux tubes might provide an effective correlative link for the entire dayside region of the solar wind interaction with the magnetopause and cusp ionosphere.

The TBL disturbances are characterized by kinked, double-sloped wave power spectra and, most probably, three-wave cascading. Both elliptical polarization and nearly Alfvénic phase velocities with characteristic dispersion indicate the kinetic Alfvénic nature of the TBL waves. Bi-spectral phase coupling could effectively support the self-organization of the TBL plasma by means of coherent resonant-like structures. The estimated characteristic scale of the ‘resonator’ is of the order of the TBL dimension over the cusps. Inverse cascades of kinetic Alfvén waves are proposed for forming the larger scale ‘organizing’ structures, which in turn synchronize all non-linear cascades within the TBL in a self-consistent manner. This infers a qualitative difference from the traditional approach, wherein the MSH/cusp interaction is regarded as a linear superposition of magnetospheric responses on the solar wind or MSH disturbances. We propose that the TBL represents an open system in a non-equilibrium steady state. In this regard we discuss the applicability of the self-organized criticality concept to the multi-scale processes in this region.

2 INTRODUCTION AND DEFINITIONS.

The International Solar -Terrestrial Physics (ISTP) program provides wide opportunities for study of the penetration of magnetosheath (MSH) plasma into the magnetosphere by means of multi-point observations. In this paper we present a case study, using data from several ISTP satellites, and present one year Interball-1 statistics, as a part of the Inter-Agency Consultative Group's (IACG) Campaign #2 on boundaries and boundary layers. Campaign #2 is described on its Web homepage: <http://www-ssc.igpp.ucla.edu/IACG/>.

Early single spacecraft observations with Heos-2 and later Prognoz-7, 8, 10 have shown that the magnetopause (MP) position and magnetosheath plasma flow structures are quite variable near the cusp, a magnetospheric region that is crucial for magnetosheath plasma entry (Paschmann et al., 1976; Haerendel and Paschmann, 1975; Klimov et al., 1986, Lundin et al., 1991; Savin, 1994).

Because of differences in the data, researchers have divided the high altitude cusp into a number of layers and regions. Since full agreement on how this should be done is not yet achieved, we will give the definitions and descriptions of the regions discussed in this paper. These regions, shown in Plate A1, are: the outer and inner cusps, the outer cusp throat (OT) and the turbulent boundary layer (TBL). The reader is referred to the papers by Smith and Lockwood (1996) and Angelopoulos et al., (2001) for a synopsis of measurements and models of the low altitude cusp. Referring to Plate A1, the outer cusp throat (red slant-line shaded region) is outside the MP, the outer cusp (blue) is just inside the MP, and the inner cusp is deeper in the magnetosphere. We identify here the MP (inner red line) as the innermost current sheet where the magnetic field turns from Earth-controlled to magnetosheath-controlled (Haerendel and Paschmann, 1975). The outer cusp is a region with three different particle populations; newly injected MSH ions, MSH ions reflected from the ionosphere, and quasi-perpendicular ions trapped in the local magnetic field minimum near the cusp (Savin et al., 1998b, Sandahl et al., 2000). There are also electrons accelerated along the field lines. The newly injected and quasi-perpendicular ions dominate over those that are reflected. This is one of the characteristics distinguishing the outer cusp from the inner cusp and from the distant mantle. The outer cusp is also characterized by moderate magnetic noise while in the inner cusp there is a similar type of noise observed primarily only at the boundaries (Pottelette et al., 1990). The outer cusp consists of the entry layer and the portion of the plasma mantle adjoining the entry layer (Paschmann et al., 1976). According to the work of

Yamauchi and Lundin (1997) the entry layer and mantle that are parts of the outer cusp form one continuous region.

At the cusp the magnetopause is indented. This indentation was first predicted by Spreiter and Briggs (1962) and then detected by HEOS-2 (Paschmann et al., 1976), ISEE (Petrinec and Russell, 1995), and Hawkeye-1 (Chen et al., 1997). Zhou and Russell (1997) found that the MP is closer to the Earth at high latitudes than at low latitudes. Interball-1 statistics show that the indentation is on the average about 2 R_E deep (Savin et al., 1998b). We call this part of the exterior cusp the outer cusp throat. The plasma in the outer cusp throat is highly disturbed and/or stagnant MSH plasma. The difference between our outer cusp throat and the "stagnation region" defined by Haerendel et al. (1978) is that the stagnation region has no specific relation to the magnetopause, as noted by the multiple arrows in Plate A1. Usually, the magnetopause can be recognized in both Polar and Interball-1 data, but when this is not the case it is better to use the term "stagnation region", rather than "outer cusp throat".

The turbulent boundary layer (TBL) is a region dominated by irregular magnetic fields and plasma flows. It is located just outside and/or at the near cusp magnetopause and has recently been found to be a permanent feature (Savin et al., 1997, 1998b, 2002, Klimov et al., 1997, Sandahl et al., 2000). Here the energy density of the ultra low frequency (ULF) magnetic fluctuations is comparable to the ion kinetic, thermal, and DC magnetic field densities. The ULF power is usually several times larger than that in the MSH, and one or two orders of magnitude larger than that inside the magnetopause. As recent studies conclude (see e.g. Belmont and Rezeau, 2001 and references therein) the strong ULF fluctuations that occur just outside of or at the magnetopause can independently result in micro-reconnection and local plasma penetration all along the magnetopause surface even without the presence of quasi-stationary global reconnection. In two case studies Savin et al. (1998b) have shown that large-scale structures (> 30 s) tend to be spatial, while for shorter time scales the temporal changes are significant. In this paper we do not separate the spatial changes from the temporal variations. We utilize the magnetic AC power related to the average plasma and field energy density in the magnetosheath as a rough measure of the strong turbulence regime. This ratio being > 0.1 corresponds to strong diffusion discussed in the percolation theory of Kuznetsova & Zelenyi (1990). Haerendel (1978) was the first to introduce the turbulent boundary layer in cusp physics in a discussion on the interaction of the magnetosheath flow with the magnetopause at the flank of the tail lobe. Examples of highly turbulent magnetic and electric fields in the exterior cusp have been reported by Paschmann et al. (1976) and Haerendel et al. (1978) from Heos-2, by Klimov et al. (1986) from Prognoz-10, by

Savin (1994) and Blecki et al. (1998), from Prognoz-8 and by Chen et al. (1997) from Hawkeye-1 data, but the referenced papers dealt neither with the turbulent boundary layer statistics nor with multi-satellite data. Only the Prognoz-8 and 10 magnetic field experiments had high enough sampling rate (1-50 Hz versus ~ 0.03 Hz on Heos-2 and Hawkeye-1) for turbulent boundary layer studies. However, the absence of 3D plasma measurements and poor statistics prevented a systematic study of the turbulent boundary layer signatures and of the TBL's role in mass and momentum transport at the high latitude magnetopause.

The main goal of this paper is to advance the achievements and explore solutions to the problems associated with the physics of the exterior cusp in the Interball era. At the same time, we have significant amounts of original results from recent analyses of multi-spacecraft data, which are obviously beyond the scope of a single paper. Thus, as a compromise, we limit ourselves in the data presentation to a fortunate multi-point case and a consideration of that case in the context of one year of Interball-1 operation. The case study presented in this paper deals with the dayside cusp and magnetosheath interface during dominant northward IMF conditions. We discuss examples of the characteristic regions at the cusp/MSH interface on the basis of the data from Interball-1 and Polar on May 29, 1996 and compare them with results of global MHD modeling of the solar wind interaction with the magnetosphere. There are a number of previous studies of this event, but they have concentrated on single spacecraft data (see e.g. Russell et al., 1998, Savin et al., 1998a, Chandler et al., 1999, and Avanov et al., 2001). In our study Interball-1 serves as the upstream MSH monitor for Polar in the TBL and for HEO-095 and DMSP in the inner cusp (see Grande et al., 1997) and ionosphere, respectively. We also add wave data to distinguish different regions and phenomena. One of the main questions we address here is whether the TBL plays a substantial role in MSH plasma penetration into the magnetosphere. We make use of the spacecraft fleet data and event-oriented modeling to determine if the antiparallel magnetic field merging (either local or remote from the cusp) is able to account for the widespread cusp, detected on this day from the ionosphere to the magnetopause over a wide range of local times. We present statistics of the high level of ULF magnetic turbulence (i.e. of the TBL) and occurrence of ion heating on the basis of one year of Interball-1 data. The statistics provide background both for the case study that is presented and for other cases discussed throughout the paper. In the second part of our paper we summarize the TBL properties, as known up to this point in time, and discuss three types of reconnection that are proposed to occur at different scales. We consider percolation of the MSH plasma as a source for the cusp and boundary layers. We compare the direct interaction of MSH flows with the indented MP over the cusp with reconnection as an alternative

source for the TBL. A scenario for three-wave resonance-like interactions in the TBL is proposed. We treat the high-latitude MP as a nonlinear distributed system with memory.

3 SITES OF MSH PLASMA PENETRATION ON MAY 29, 1996

In Plates A2 and B1 we present multi-instrument Interball-1, Magion-4 and Polar data on May 29, 1996. In Plates A3-A5 one can see the Interball-1 and Polar orbits relative to the cusp- MSH interface, the details of these Plates are discussed below. The top panel (a) of Plate A2 shows protons perpendicular to the satellite spin axis and Sun-Earth line measured by the PROMICS-3 instrument, the ion temperature T_i is over-plotted by black line. Panels b and c show the magnetic field in the GSM coordinate system. Panel d gives the different components of the energy density; the total energy density, E_s , black shading, and its three components, the thermal energy density, $E_{\text{thermal}} = 1.5 n k T_i$ (where n - plasma density, T_i - ion temperature), the kinetic energy density, $E_{\text{kinetic}} = 0.5 n M_i V_i^2$ (yellow shading, where M_i and V_i - ion mass and velocity) and the magnetic energy density, $E_m = \mathbf{B}^2/8\pi$ (dark gray shading). Panel e displays GSE V_x and V_z components of ion velocity from the MHD model of Fedder et al. (1997) (black trace) and measurements by SKA-1 ion spectrometer (see details of the plasma data in Avanov et al., 2001), which are red colored with gray shading. Panel f shows the power contained in the magnetic field variations, D_f , and the standard deviation of the magnetic field magnitude, D_m . D_f is obtained by taking the sum of variation powers in B_x , B_y and B_z . Then we use the relation $1 \text{ eV} \sim 2.49 \text{ nT}^2$ to express D_f/D_m in energy density units. The variations are calculated over two minute intervals with the interval shifts of 30 seconds. Panel g gives Fourier spectrogram of the magnetic field with sampling rate 4 Hz and the proton cyclotron frequency (blue line). Panel h, finally, shows magnetic spectra from Interball-1's companion satellite, Magion-4, in the range 20-2000 Hz during a period when Interball-1 observed turbulence.

The different regions depicted in Plate A1, which were passed by Interball-1, are marked at the top of Plate A2. Until 0220 UT Interball-1 was in the inner cusp. At ~0230 UT the mantle was encountered. Particle fluxes were fairly weak and had no earthward component (not shown). The outer cusp (OC) boundary was approached at about 03 UT, which is indicated by increased particle fluxes and wave activity. At 0317 UT the MP was crossed. This can here be determined from the sign change in B_z , which went from negative inside the magnetosphere to positive in the

outer cusp throat (OT). Also the sign of B_x changed. At the magnetopause current sheet the thermal energy density was the main component in the total energy density, while there was a dip in the magnetic energy density. The period from 0315 to 0319 UT represents a typical example of a turbulent boundary layer at the OT edge. At 0317 UT in Plate A2 maxima are seen (marked by black shadowing), in T_i , thermal and total energy densities and magnetic field spectra. A characteristic feature of the TBL is the dominance of incompressible waves resulting from the fact that total wave power, D_f , is several times higher than the magnetic field magnitude standard deviation D_m (gray shadowed on panel f; cf. Savin et al., 1998b). The total energy density measured in the magnetosheath outside the cusp was about 30 keV/cm^3 , the magnetic wave power in the TBL reached 6 keV/cm^3 and thus the ratio between the two was $D_f/E_s \sim 0.2$ (i.e. exceeds the strong turbulence limit of 0.1, see previous section).

There is an interesting feature between the MP and the rotational discontinuity (RD, see details in Savin et al., 1998a) in Plate A2(d): the kinetic energy density (yellow shading) exceeds the thermal one. That means supersonic magnetosheath flow just outside magnetopause (the sound Mach number $M_s \sim 2$, while the Alfvénic Mach number $M_A \sim 0.9$). This picture resembles the 'Laval nozzle' cusp model (see Yamauchi and Lundin, 1997). The model scheme is reproduced on Insert A of Plate A2. The blue thick arrow shows the inferred Interball-1 orbit. We would like to mention the general agreement between the model and measured velocities on panel e, we discuss this matter in a following section in details. The measured V_z demonstrates negative wave train and then tailward acceleration at and just after MP. V_x is generally negative that corresponds to streamline of MSH flow around MP outside it and to the mantle inside. As it has been discussed in Savin et al. (1998a), the mantle existence during northward IMF is unusual and can imply the MSH plasma penetration upstream Interball, while the positive wave train in the measured V_x prior/at MP clearly point on the reconnection downtail, V_z in the wave train agrees with the latter too.

Polar data are presented in Plate B1. Panel a shows the magnetic field; panel b displays GSM V_x and V_z components of ion velocity from model (see Fedder et al., 1997 for details) and vector velocities from the moments of measurements of protons by TIMAS spectrometer, V_x and V_y are red/ blue shadowed for positive/ negative values. Panel c shows the total energy density, E_s , (underneath the black shading), the thermal energy density, and the magnetic energy density (yellow shading). Panel d gives the average ion energy T_i and average electron energy T_e from HYDRA. Panel e shows the magnetic field variations calculated in the same way as on panel f of Plate A2. Panels f, g, h and i give electric and magnetic spectrograms. The Polar data differ from

those of Interball-1 in Plate A2 by extended duration crossings of the intensive part of the turbulent boundary layer. The TBL is seen as increases of the wave power, D_f , of 8-40 times that of the stagnant MSH. The TBL threshold ($D_f = 400 \text{ eV/cc}$, $\sim 13 \text{ nT}^2$, see panel e) is about two times higher than D_f in the stagnant MSH. $D_f \gg D_m$ displays strong dominance of the transverse waves over the compressible ones in the TBL.

On the Polar outbound leg there is a gradual rotation of the average field direction immersed in the high level TBL (0400- 0445 UT). The main MP current sheet at 0408 UT is rather weak (see the B_z change on panel (a)). In the TBL wave power reaches 15-20 % of the total density E_s at 0510 UT, or of the simultaneous Interball-1 one in MSH, respectively. The 'magnetic bubbles' are identifiable by the spiky drops in $\mathbf{B}^2/8\pi$ and $|\mathbf{B}|$ (green shadowed in Plate B1, panel c). T_e , T_i and the thermal energy E_t rise in TBL by factors of 2-4 compared with their minimums at 0500 UT (black and brown shading in Plate B1), or with Interball-1 data at 04 UT (blue shading for T_i). The MHD model predicts even lower T_i value (green shading) at this time (black arrow in Plate B1(e)). The TBL with higher turbulence level is on the Polar inbound into the polar cap at 0616-0708 UT. T_i and E_t rise is a factor of 3-6, D_f reaches 25-33 % of the MSH E_s , in 'magnetic bubbles' $|\mathbf{B}|$ drops down to fractions of nT. Minimum T_i is ~ 2 times higher than both the MHD model one and that in the unperturbed MSH at the same time. This could result from heating both in the TBL (if the MSH plasma enters then leaves TBL) or at the interface between the streaming and stagnant MSH. Note also the remarkable wave train in the velocity at 0640- 0700 UT data (panel b of Panel B1). We devote a special section to the detailed study of this period with the unpredicted by the MHD model nearly Alfvénic velocity jets.

3.1 TBL WAVE SIGNATURES

Romanov (1998) and Savin *et al.* (1998b) have demonstrated that in the TBL the incompressible elliptically polarized waves are dominating at frequencies less than the proton gyrofrequency. But unlike the linear Alfvén waves, the TBL contains 'magnetic bubbles' with heated plasma and low total magnetic field inside. Wave power D_f in TBL exceeds 30% of the ion energy density in MSH, (Plates A2 & B1), the thermal density E_t rises up to four times. An Interball 'turbulent zone' encounter on the tail field lines has been presented by Klimov *et al.* (1997). The electric and magnetic field spectrograms demonstrated very clear TBL in the magnetic field, while the electric field spectra also had rather high amplitude just inside MP. The same type of behavior one can see

in the Polar/PWI data near the dayside TBL on May 29, 1996 in Plate B(f-i). The spectrogram Ez (panel f) demonstrates spiky activity in TBL at 0400-0445 and 0617-0708 UT, simultaneous with the ULF magnetic bursts on panels (g-i). In the polar cap at 0755-0810 UT there are the electric field bursts, similar to that in TBL, without corresponding magnetic field ones. The TBL magnetic bursts are quite wideband, reaching the electron cyclotron frequency (panels g). In between the TBL and at their outer borders one can see spectral maxima from 200 to 1000 Hz, which correspond to the "lion roars", a characteristic feature of the MSH encounters (Anderson *et al.*, 1982). The most prominent "lion roars" maxima are located near 300 Hz, that corresponds to the Magion-4/SAS data at 0400 UT in the near-MP MSH (panel h in Plate A2), Magion-4, being at (4, -3.6, 8.7) Re in GSM frame, is ~ 1500 km ahead Interball-1 along the orbit track (cf. Blecki *et al.*, 1998). Thus the Polar/PWI data supports the Polar encounter of the stagnant MSH on May 29, 1996 in between the TBL. In the lowest frequency band the ULF waves have maximum 0.01-0.1 Hz, that agrees both with Savin *et al.* (1998b) for April 21 and 2, 1996 with IMF Bz < 0 (for the major part of TBL) and with earlier reported characteristic plasma fluctuation periods from Heos-2 (Haerendel, 1978). The clear emission slightly below the He++ cyclotron frequency is seen in Plate A2(g) at 0256-0304 UT. Weak emissions close to proton cyclotron frequency Fcp+ can be recognized at 0305-0313, 0335 and 0357 UT (cf. Klimov *et al.*, 1986, Savin 1994, Klimov *et al.*, 1997). These ion cyclotron emissions outside TBL indicate that non-equilibrium ion distributions are generated in the TBL (cf. Belova *et al.*, 1991, Treumann *et al.*, 1995).

To compare the ULF waves in the central TBL, near the boundary between the mantle and LLBL field lines and in the low altitude cusp we present the characteristic electric and magnetic Fourier spectra in Figure 1A. The full upper curve displays the sum of the powers of 3 Polar magnetic field components (marked 'B'), the lower gray shadowed curve shows that of electric field components at 0700-0702 UT in TBL (see Plate B2 for the survey). The electric to magnetic field amplitude ratio provides a proxy for phase velocity (marked by 'E/B'). The Alfvén speed V_A is shown by the horizontal thick light line. $E/B \sim V_A$ for the dominant waves in TBL. We refer to them as Alfvénic Nonlinear Vortices. The magnetic vector hodographs in minimum variance frame in Figure 2 illustrate their vortical nature. The first vortex-like signal from Interball-1 in Figure 2A corresponds to the Vx and Vz sunward wave train in Plate A2(e). For the planar geometry the wave vector direction is in the minimum variance direction Bk (0.64 -0.72 0.25). Avanov *et al.*, [2001] calculated the de Hoffmann- Teller velocity for the middle of the vortex interval of $V_{HT} = (32 -178 98)$ km/s. From this we estimate the vortex space scale $L \sim 2\pi/k$. For the Alfvén wave in the time domain frequency in the spacecraft frame $f' = f + (\mathbf{k}/2\pi * \mathbf{V}_{HT})$. In the

plasma frame $f \sim k V_A / 2\pi$ (see Figure 1A). We find for typical parameters $L \sim 650$ or 1700 km depending on the \mathbf{k} sign. For pure spatial structure with $f = 0$, $L \sim 520$ km. Thus, one can accept $L \sim 1000$ km as a reasonable value for the vortex scale. It represents several tens of ion gyroradii for the measured plasma parameters.

Figure 2B shows an example of a magnetic field vortex-like structure from the Polar TBL inside the interval of the Polar spectra in Figure 1A. Figure 2C displays the more irregular behavior of the electric field at the same time. To check if the TBL waves in Figure 1A can be regarded as spatial structures passing Polar, we approximate the E/B ratio by the dispersion curve of the kinetic Alfvén waves (KAW). Near Polar apogee, Stasiewicz et al. (2001) have shown that the KAW with the speed V and ion gyroradius ρ_i should result in E/B in the frequency (ω) domain in the satellite frame of reference as follows:

$$(E/B)^2 \sim V_A^2 (1 + (\rho_i \omega / V)^2) \quad (1)$$

We present the calculated E/B from (1) by dashed line in Figure 1A for $V_A \sim 70$ km/s, $\rho_i \sim 60$ km and $V \sim 150$ km/s (cf. Plate B1). The average measured E/B behavior is close to the expected for the KAW one, while at frequencies over 1 Hz high amplitude fluctuations around the average value are seen. These fluctuations correspond to the random ones on the electric field hodogram in Figure 2C, i.e. most probably due to the electrostatic waves in the proton gyrofrequency vicinity. If our interpretation of the waves as KAW is true, we can roughly re-scale the E, B and E/B spectra in Figure 1A into the space domain, as shown in Figure 1A above the horizontal axis by L (in km). Note that for the typical TBL frequency of 0.1 Hz the inferred scale is close to that of Interball, namely to 1000-2000 km. Thus different methods provide compatible scales for the vortex-like fluctuations in the TBL.

Returning to the Figure 1A we mark by the squared white ‘G’ one of the strongest electric field spectrum in the TBL-like region, which has been detected aboard Geotail on August 27, 1995 during highly disturbed MSH conditions ($Df > (15 \text{ nT})^2$ at (4.5; 10.4 - 4.2) Re in GSM frame, see also Figure 6 for the position of this crossing marked by squared gray ‘G’). The electric field AC power for this disturbed case is by more than order higher than that of Polar in TBL on May 29, 1996. That fact indicates that in the disturbed SW conditions the fluctuation power near MP can be much higher than in TBL on May 29, 1996 representing a case with highly compressed magnetosphere by the dense MSH (see Figure 4 below). We suggest that the higher-level disturbances correspond to dynamic interactions of SW discontinuities with MP.

Just inside MP the magnetic wave power drops sharply (see Plates A2(f,g) and B1(e)), so that the waves can hardly heat the core proton and alpha particles by their own energy. Instead, they are a

good indicator of the plasma non-equilibrium state and represent the mean for the energy redistribution between the particle species and for diffusion in the velocity space. The Polar case of the thick MP at about 04 UT is an exception: at 0338-0408 UT the D_f is higher than usual (cf. Savin *et al.*, 1998b, and Plate B1(e, g- i) at ~0710 UT). Interball-1 data also display the enhanced wave power at 0300-0315 UT where the quasi-perpendicular, reflected and ‘fresh’ injected ions are mixed and the strong waves are generated in such extremely non-equilibrium plasma (see Plate A2). In the deeper weak cusp and mantle at 0200-0255 UT only weak magnetic spikes are seen, indicating mainly on the plasma flow gradients (panel f).

At the lower altitudes in steady situations only electric field variations are usually seen. A characteristic example for the low altitude cusp variations from Interball-2 was observed on January 22, 1997 and is shown in Figure 1A by the curve marked by circled ‘A’ (at 0058 UT at height of 2.3 R_e). While its absolute power exceeds that of Polar TBL (gray shadowed), the scaling factor in the divergent Earth's magnetic field reduces the low altitude equivalent power to more than order of magnitude less at the Polar apogee height. During geomagnetic disturbed conditions Pickett *et al.* (1999) also reported the specific ULF wave activities in low altitude cusp in conjunction with the energetic particle bursts. Unlike TBL, the magnetic fluctuation power deep in the cusp is negligible as compared with the local DC magnetic field pressure.

Now we would like to make use of the simultaneous Interball and Polar magnetic field measurement in different regions near MP. A poorly explored problem is how the MSH –born fluctuations influence the TBL turbulence. We present wavelet spectrograms of the GSM By components from MSH (Interball) and TBL (Polar) at 04-05 UT in Figure 3A and 3B. Wavelet analysis is a powerful tool to investigate turbulent signals and short-lived structures. In order to examine the transient nonlinear signal in the TBL we have performed the wavelet transform with the Morlet wavelet:

$$W(a, t) = C \int \{f(t_i) \exp[i 2\pi(t_i - t)/a - (t_i - t)^2/2a^2]\} dt_i \quad (2)$$

where ‘C’ has been chosen so that the wavelet transform amplitude $|W(a, t)|$ is equal to the Fourier one (see Consolini and Lui, 2000 and references therein for details). This wavelet shows the single peak at the frequency $f = 1/a$, a wavelet characteristic scale may be read as representing a frequency $f = 1/a \pm f/8$. We use SWAN software from LPCE/CNRS in Orleans for the wavelet analysis. The wavelet spectrograms in Figure 3A and 3B clearly outline wave trains (i.e. isolated maxima) at different frequencies simultaneously that indicates on the multi-scale nonlinear processes (cf. Plates A2(g) and B1(i) where fast Fourier has been used). The linkage between the maxima represents a feature of cascade processes, the direct/ inverse (i.e. high or low frequency

fluctuations appear first) cascades might be inferred. While the spectra character in MSH and TBL seems to be similar, no detailed correlation is seen especially for the frequencies > 0.03 Hz and at 0450-0500 UT. Note also the color scale difference: the TBL spectra are of about an order of magnitude more intensive. We have found that the general correlation of the B_y components on Polar (in TBL and stagnant MSH) and Interball (in the nominal MSH) on the time intervals of 0.5-1 hour is poor (< 0.2), while for disturbances such as MSH discontinuities the correlation can reach 0.7 on intervals of the order of 5-10 minutes, no well-defined time delays can be found (i.e. correlation functions are flat on intervals of several tens of seconds). The only longer disturbance on Polar at 05:26-05:45 UT have the respective counterpart in the Interball post shock data (not shown) with correlation coefficient of 0.6 and the clear time delay of 925 s.

For quantitative comparison of the wave spectral features we present the characteristic integrated Morlet wavelet spectra in Figure 1B. We have chosen two intervals with Interball-1 as upstream monitor in the nominal streaming MSH and Polar in or just over TBL: (1) 0409- 0439 UT with similar character of the wavelet spectrogram (Figure 3a and 3B) and (2) 0500- 0545 UT with Polar just outside TBL (or even at its border, see Plate B1(e-i)) and Interball-1 in the disturbed MSH just downstream bow shock (BS, see Savin et al., 1998a). Comparison of the magnetic spectra shapes in the TBL and stagnant MSH over TBL versus the nominal flowing MSH from simultaneous Polar and Interball-1 data shows that the low frequency disturbances (at 0.001-0.002 Hz) can be transmitted throughout the MSH from downstream the BS. It is seen from both the coincidence of the MSH and TBL spectral powers (asterisks and crosses) and existence of the spectral peak at these frequencies throughout MSH in two other spectra. The mechanism of the power amplification at these frequencies over TBL is unclear (see dark shading of the power difference in Figure 1B).

Plate A

Plate B

There are several opportunities for that:

- (a) amplification at the discontinuity (shock?) between stagnant and flowing MSH;
- (b) amplification due to convergence of the outer cusp throat; (c) accumulation of the permanently inflowing disturbances in the stagnant OT; (d) out-flowing of the waves from TBL (note the higher frequency of the peak near 0.001 Hz on Polar at 0500- 0545 UT in Figure 1B). As for the disturbances at frequencies > 0.01 Hz, its occur to dissipate downstream bow shock as their power near MP is lower than near the BS (the respective difference is light-shadowed).

Figure 1A

Figure 1B

The most characteristic TBL waves at 0.005-0.5 Hz happen to have the characteristic kinked spectral shape and slopes (note the higher power and different shape in this frequency band of the spectrum marked by crosses in Figure 1B). It is similar to the near-Earth neutral sheet during substorms, the lower slope of about 1 might be attributed to the flickering noise (see e.g. Zelenyi and Milovanov, 1998 and references therein). In the TBL this expectation of the intermittent quasi-coherent structures is realized in Alfvénic nonlinear vortices (ANV), which are displayed in Figure 2 (see discussion above). The spectral power here is much higher than that of fluctuations in the flowing and stagnant MSH, the spectral shape is different: the kinked shape with the slopes of 1-1.5 and 2-2.6 are the characteristic TBL ones, while spectral peak at lower frequencies might also appear (cf. the dark-shadowed spectrum over TBL in Figure 1B). A substantial TBL feature, which coincides (we suppose by chance, see discussion in section 6.5 below) with the simultaneous MSH one in Figure 1B, is the frequency of the kink (asterisks and crosses).

Figures 2A- 2C

To verify the local TBL origin of the turbulence, at least partial, we study Poynting flux on the interval of the Polar data in Figure 1A (0700- 0702 UT). In Plate B2 we present the Poynting flux angular distribution, its relative magnitude is shown by contours with increment value of factor 2. The blue shading corresponds to the maximum Poynting flux magnitude. The GSM axes are labeled in circles, the Z (-Z) axis corresponds to the upper (bottom) horizontal line. The direction of the average magnetic field is marked by crosses, the median frequencies of the intensity maxima are given in mHz. Note that the characteristic maxima have frequencies of 50-60 mHz, that corresponds to the most prominent maxima in the power spectra in Figure 1A. Spectral analysis of the Poynting vector and its decomposition on the differently propagated waves has been performed using the method of Romanov, (1998). In the interval under study negligible Poynting flux has positive projection on the average magnetic field (that is under the curve, showing the perpendicular plane to magnetic field in the Plate B2). Instead, the maximum electromagnetic energy is flowing both antiparallel to magnetic field (close to the inclined blue cross and nearly along MP downstream the cusp (i.e. ~ in the middle between the -X, Y and Z axes). The fluctuation power has characteristic magnitude for the TBL (see Plate B1(e-i)). So, we conclude that a process poleward Polar has comparable power with the processes at the origin of

sunward jets at 0645- 0700 UT (see Plate B1(b), Figure 4 and related discussions below). This process, probably small-scale reconnection at the cusp- MSH interface, is certainly the inherent TBL one, i.e. the high level electromagnetic energy can't originate from the remote reconnection site (see RRS in Plate A3 and A4 and related discussions below) at 0700- 0702 UT, on the time interval of Figure 1A and Plate B2.

Thus, we conclude that for the case under study the substantial disturbances are generated in TBL, having character different from the waves in both near-Earth MSH and downstream bow shock. This inherent interaction is thought to be modulated by the MSH flow disturbances and discontinuities.

3.2 TBL: RANDOM OR ORGANIZED?

Now we address the question if the sunward flows, MP-like current sheets and 'diamagnetic bubbles' in Plates A2 and B1 are driven by random SW/MSH disturbances or its follow some kind of correlated or coherent behavior, at least during rather stationary SW periods. In other words: can the local TBL processes (including reconnection-like) be regarded as a collective multi-scale interaction pattern? In Figure 1B we have already demonstrated a feature of self-organized processes, namely power-law kinked spectra in TBL (curve marked by crosses) but e.g. the streaming MSH could have the spectra of similar shape (curve marked by asterisks). To get further insight into the problem we show in detail Polar parameters in the inbound TBL (Figure 4) and analyze B_z component by the Morlet wavelet transform, wavelet correlation time and bicoherence (Plate B3- B5).

In Figure 4 we blow up TIMAS mass-spectrometer proton moments and magnetic field in TBL at 0640- 0700 UT: the parallel (upper black) and perpendicular (violet line) temperatures (linear scale at the right side, the difference between the parallel and perpendicular temperatures is shadowed by violet color), the ion velocity $|\mathbf{V}|$ (upper gray shading), GSM V_y and V_z (dotted black and dashed red lines), V_x (lower green shading) and the density N_i (lower blue shading, linear scale at the right side). At the bottom of the upper panel: characteristic Alfvén speed V_A in the disturbed MSH (gray shading) and in the velocity jets (marked by arrows). The bottom panel displays GSM B_z (linear scale at the right side) and $|\mathbf{B}|$ (yellow shaded). The B_z is generally positive in the MSH and negative in lobes (cf. Plate B1(a)). Velocity sunward jets (up to $|\mathbf{V}| = 285$ km/s) are pointed

counter-stream (i.e. $V_x > 0$, $V_z < 0$), they clearly correlate with the minima in N_i and negative (magnetospheric-like) B_z . Another characteristic jet feature is parallel heating. Note also the general excess of the parallel temperature in the region of jets and ‘bubbles’ at 0645- 0657 UT: this strongly suggests that mirror waves can’t account for the ‘diamagnetic bubbles’ formation as for the mirror instability the perpendicular temperature should exceed the parallel one (see e.g. Stasiewicz et al., 2001 and references therein). Angles between the magnetic field and three velocity jets, marked by arrows at the bottom, are respectively 16.5, 16.5 and 29 degrees (from left to right). Thus, the jets are practically field-aligned, being accelerated till velocities between the local and MSH Alfvén speeds. The presence of these jets, along with the ‘diamagnetic bubbles’ and parallel proton heating, strongly infers the field-line reconnection downtail of the Polar position (cf. Savin et al., 1998a, Stasiewicz et al., 2001). The density N_i anti-correlates with the $|\mathbf{B}|$, this might be regarded as random MP crossings, (cf. Urquhart et al., 1997). On the other hand, the velocity wave train in the Figure 4 is rather regular and remarkably resembles that of Interball in Plate A2(e). One possibility is that both of them result from the downtail RRS, while for Polar it isn’t reproduced by the global MHD model (see Plates A2, A4, B1). In this case the reason for the patchy character of the reconnection might be in the high flow velocity near RRS (with nearly Alfvénic and at some times supersonic velocity, see Plate A2 and discussions above), which prevents occurring of the stationary reconnection (see La Belle-Hamer et al., 1995).

We would like to discuss also another data explanation that suggests e.g. the local TBL reconnection, Alfvén resonator etc. (cf. Savin et al., 1998a, 2002, Stasiewicz et al., 2001). In Plates B3- B5 we present the results of detailed wavelet analysis for the chosen TBL interval. Plate B3 shows Morlet wavelet spectrogram for 0.00156- 0.05 Hz. It is similar to that of Figure 3B: the isolated maxima correspond to wave trains, they constitute the cascade-like chains that are tentatively shown by black curves with respective circled numbers. The inverse (1,3) and direct (2,4,5) cascades could be inferred, the most prominent ones are marked by the numbers 2 and 5. The main wave train, visible in Plate B1(b) and Figure 4 throughout the TBL at 0640- 0710 UT, corresponds to the long stable maximum at ~ 3.3 mHz in the Plate B3. The maximum at 1.6- 1.7 mHz is visible even inside magnetosphere. We have checked that the V_z and V_x spectrograms have similar character to that of B_z in Plates B3, while for different components the different maxima are most explicit.

To investigate the wave train coherence we utilize the wavelet correlation time. For that calculation the wavelet coefficients are considered, at every frequency, as a time history signal. This corresponds to the output of a low bandwidth filter centered on the analyzing frequency. A

correlation analysis is performed over these new signals, taking into account a possible non-stationary of the signals. The input series is the time variation of the wavelet coefficients $C(k,m)$. The function depends on the beginning time of the analysis t . At every discrete frequency m , the correlation function $R_c(t,l,m)$ is computed on a small moving time window:

$$R_c(t, l, m) = \frac{1}{N_l} \sum_{n=iN_l}^{(i+1)N_l-l-1} (C(n,m) - \mu_c) (C(n+l,m) - \mu_c)^*, \quad 0 < l < l_{\max}$$

where N is the number of samples used to compute the correlation function and l_{\max} is the maximum number of lags. The variable μ is the mean value of the coefficients and $*$ means the complex conjugate operation. A time overlapping can be done. The correlation time is then estimated by the relation:

$$\tau_c(t, m) = \gamma / T_f \sum_{l=0}^{l_{\max}} |R_c(l, m)| / R_c(0, m)$$

where T_f is the period of the analyzed frequency ($T_f = 1/f$). Then, the result is expressed in terms of number of the periods (by selection of appropriate $\tilde{\alpha}$). In Plate B4 we present wavelet correlation time in the range of 2.5-80 mHz for the TBL and MSH crossing by Polar, Insert A displays that of Interball-1 outbound MP/TBL crossing for comparison. The TBL on Polar is specified by the highly coherent (correlation time ≥ 3 periods) wave trains, visible at the low frequencies for several sub-intervals of the analysis.

The most prominent feature in the Polar TBL is a coherent structure at ~07 UT (marked by an ellipse with the circled label A), this is namely the wave train at ~ 3.3 mHz outlined in the discussion of Figure 4 and Plate B3. The higher frequency coherent signals (e.g. at 17, 23, 35, mHz, cf. Plate B3) are not specific only for the TBL. The inbound TBL at ~ 0430 UT is also characterized by the coherent wave trains but at several frequencies simultaneously (~ 2.8, 4.5, 6.7 and 8.5 mHz, cf. Figure 3B). One hardly can guess the coherent wave trains from waveforms or Fourier spectra in Plate B1(h,i) at ~ 0430 UT (we checked that the corresponding maxima are seen on V_x and V_z wavelet spectrograms as well). While period of ~ 3 mHz signal on Interball (Insert A) is short (of the order of the TBL crossing time, see Plate A2), the wavelet analysis segregates the correlation time at this frequency (> 2 periods) relative to the neighbor ones. This is rather interesting as Interball and Polar crossed the outbound/ inbound TBL at about the same X and Z (see Plate A3), while at different times and at symmetric Y relative to the noon. The difference in

the duration of the TBL encounters is, most probably, due to Interball crossing of the current sheet ~ along the normal, while the orbit of Polar is nearly elongated the MP current sheet (see Plates A4- A5). The coherent Interball signals throughout MP/TBL crossing are visible at ~ 5 and 18 mHz, the 5 mHz one corresponds to the well visible V_x/V_z wave train in the Plate A2(e). Thus in both cases the coherent magnetic and velocity signals are seen for a long time throughout the cusp/MSH transition. That is different from both usual concepts of stationary reconnection and random reconnection bursts: in the former case the repetitive flows should not be seen during ~ steady solar wind conditions, in the latter case the bursts should be random instead of coherent.

We would like to do further test for possible self-organization in the TBL processes: we use the wavelet-based bicoherence to check if the wave trains at different frequencies really constitute the coherent interactive system with multi-scale features. In the SWAN software, we use for the wavelet analysis, the bicoherence is defined as:

$$b^2(a_1, a_2) = |B(a_1, a_2)|^2 / \{ \sum |W(a_1, t_i) W(a_2, t_i)|^2 \sum |W(a, t_i)|^2 \} \quad (3)$$

with $B(a_1, a_2)$ being the normalized squared wavelet bi-spectrum:

$$B(a_1, a_2) = \sum W^*(a, t_i) W(a_1, t_i) W(a_2, t_i) \quad (4)$$

the $W(a, t)$ is the wavelet transform defined by equation (2) and the sum is performed satisfying the following rule:

$$1/a = 1/a_1 + 1/a_2 \quad (5)$$

which correspond to a frequency sum rule for the 3-wave process, $f = f_1 + f_2$.

The bicoherence has substantial value if three processes, with the highest frequency being the sum of the rest two, are phase-coupled (cf. Consolini and Lui, 2000). The simplest such case is the harmonic generation due to quadratic non-linearity, namely the second harmonic generation with $2f = f + f$, the third harmonic one with $3f = 2f + f$ etc. The harmonics are present in any nonlinear wave pulse and do not represent phase coupling of the different waves. We assume that the dominant nonlinear process in TBL is 3-wave decay (or junction) as the most powerful nonlinear wave process (excluding the harmonics), which requires the third-order non-linearity in the system. We wouldn't discuss here the weaker higher-order nonlinear effects, which also might contribute in the TBL physics.

In Plate B5 we present bicoherence spectrogram for B_z SM in the Polar inbound TBL on May 29, 1996, 0640- 0710 UT, i.e. from nearly the same core TBL intervals as the spectra in Plate B3. The frequency plane (f_1, f_2) is limited by the signal symmetry considerations and by the frequency interval of the most characteristic TBL slope of ~ 1 in the Figure 1B. As we mentioned in the

previous paragraph, the bicoherence in the TBL displays the second and higher harmonic nonlinear generations and, most probably, three-wave processes with the cascade-like features, that is visible at $f_A \sim 0.003$ Hz (i.e. at the coherent wave train labeled by 'A' in the ellipse in Plate B4). We assume the cascade signatures in the Plate B5 when the bicoherence at the sum frequency, $f = f_1 + f_2$, has comparable value with that of point (f_1, f_2) . In the case of the horizontally-spread maximum, it implies that the wave at sum frequency interacts with the same wave at the initial frequency (f_A in our case) in the following three-wave process: $f_3 = f_A + f$ etc., the initial wave spectrum can be smooth resulting in the continuous bi-spectral maximum. Most characteristic frequencies, which one can see in Plates B3 and B4 (e.g. $\sim 4.5, 6.7, 18, 23, 36$ mHz), are also proved to participate in the multi-wave coherent processes that give maxima in Plate B5. E.g. the following processes could be inferred: cascade $f_A + 23 = 26.3$ mHz, $f_A + 26.3 = 29.6$ etc. till ~ 100 mHz; $4.5 + 18 \sim 23$; cascade $6.7 + 23 = 29.7$, $6.7 + 29.7 = 36.4$, $6.7 + 36.4 = 43.1$ mHz. Another set of nonlinear processes is related with the harmonic generations and their further interactions: on the spectrogram diagonal 3 strongest maxima are close to the first, second and fourth harmonics of the 'resonant' frequency f_A , the respective processes are labeled in the figure, including the third harmonic generation. Further multi-wave interactions of the harmonics could be inferred as well: $1.5 + 2f_A$ (labeled at the bottom); cascade $2f_A + f$ etc., $4f_A + f$. Note from the Plate B3, that the 1.6 mHz signal penetrates the magnetosphere) that could imply detecting of long period surface waves (cf. Savin et al., 1998b, Sandahl et al., 2000). Both 3 and 1.5 mHz maxima are present also in the Interball bi-spectra near the MP (not shown). While the process identifications are not unique (e.g. four-wave modulation instability might be involved etc.) we certainly encounter very complex picture of furcated multi-frequency (i.e. multi-scale) coherent interactions, which strongly indicate on the cascades, based on the 'resonant' frequency f_A , seen in plasma parameters in the Figure 4 as well. As for the wavelet analysis of plasma moments, we should note that the number of points in the TBL is too small for the wavelet correlation time and bicoherence determinations, while wavelet spectrograms look quite similar to that of magnetic

Figure 3

Figure 4

Figure 5

field.

Inspection of the bicoherence spectrogram for the Polar outbound TBL in Plate B6 (Bz SM component, 0414- 0444 UT, the format is the same as for Plate B5) confirms the complex coherent picture of the TBL interactions. The respective frequency of the main cascade is close to the lowest one in Plate B4 at ~ 0430 UT, i.e. $f_B \sim 2.6$ mHz, while the $2 f_B$ -signal is weaker. Similar to the Plate B4, the outbound bi-spectrogram displays coherent processes at several frequencies: the low frequency cascade (horizontally interconnected maxima) starts at f_B then at $f_k \sim 30$ mHz (horizontal axis) shifts to $f_l \sim 4.5$ mHz (vertical axis) and for $f_k > 70$ mHz both cascades at f_B and 4.5 mHz co-exist. Note, that 4.5 mHz is close to the second from the bottom maximum at 0430 UT in Plate B4; the next coherent process with maximum at ~ 7 mHz in Plate B4 probably contributes a lot into the most prominent maximum in Plate B6, labeled ' $4 f_B + 4 f_B \sim 8 f_B$ '. The process ' $f_B + 7$ mHz' has also well-seen maximum on the bi-spectrogram along with the second harmonic nonlinear generation: $7 + 7 = 14$ mHz. This second harmonic in turn looks to interact: $14 + 35 = 49$ mHz. The lower frequency bi-spectra in Plate B5 reveal also strong nonlinear interactions at ~ 1.5 mHz, i.e. close to that in Plate B3, which penetrates inside MP (see discussion of Plate B3 above). Despite differences in Plates B4 and B5 the main cascade-like nonlinear interactions look very similar on both, the main cascade is synchronized by low ('resonant') frequencies throughout the wide frequency band.

Thus, the results of the modern wavelet data analysis strongly indicate that the TBL fluctuations are highly coherent, multi-scale and organized in cascades of nonlinear interactions. The chosen coherent wave trains occur to synchronize the interactions throughout the TBL, i.e. a kind of over-TBL resonance (cf. 'Alfven resonator' assumed by Stasiewicz et al., 2001).

4 COMPARISON WITH MHD MODEL

Results of the global MHD modeling for May 29, 1996 with the SW data as an input (see Fedder *et al.*, 1995 for details) are presented in Plates A4, A5 and Figure 5. The distribution of the currents perpendicular to magnetic field (J_{perp}) in the noon meridian plane in SM coordinates are depicted in Plate A4 by the color scale. Also shown are the projections of the Polar and Interball-1 orbits onto that plane (Polar crossed this plane at 0530 UT). The dayside low latitude MP and bow shock (BS) are easily seen in the J_{perp} maximum, while at higher latitude the MP current splits into 3 branches. The sunward one, being an extension of the dayside depletion layer, might interfere

the MSH flow to reach the outer-cusp-throat dent (Savin *et al.*, 1998a). It is difficult to say if the gap between the 3 current branches (just over the Polar orbit crossing with the '40/cc' boundary at ~0320 UT) provides direct access ('cleft') for the MSH plasma into cusp. The current gradients near the spacecraft orbits should cause current drift instabilities (see e.g. Vaisberg *et al.*, 1983 and references therein), that provide a source for the TBL waves. Note, that the TBL crossings by Polar correspond to the J_{perp} maximum, the stagnant MSH encounter represents sliding along the current maximum border. The broadness of the maximum current sheet itself is believed to be due to MHD (= large scale > 3000 km) waves, which are reproduced by the model. The MP indentation is seen as the lag between 'smooth MP' (see e.g. Sibeck *et al.*, 1991 model) and the current sheet maximum. Its depth (~ 1.5 R_E) is typical for the outer cusp throat (Savin *et al.*, 1998b). The model-determined position of the 'remote' (from the cusp) reconnection site (RRS) is shown in Plate A4 by white squared cross. The model inward boundary of the MSH plasma with density > 40/cc is shown by thick black-and-white dashed line (see Figure 5 in Russell *et al.*, 1998). Intersection of the Polar orbit with this model boundary agrees with the outer cusp encounter by Polar at ~ 0320 UT, as it is seen from rise of the model V_x/V_z in Plate B1(b).

Polar returns inside MP at 0708 UT, which is reproduced by the MHD model with about 10 minute delay. The delay is seen by comparing the V_x/V_z vanishing at the right part of Plate B1(b) with the final B_z transition to the negative value in Plate B1(a). This delay seems to be characteristic for the total reproduced interval (see e.g. the model V_x sign changes at ~0420 and 0520 UT relative to the measured V_x ones). The measured magnetic field displays substantial discrepancy at the inbound MP (see Figure 4 in Russell *et al.*, 1998) due to inability of the model to reproduce sharp gradients (< 1000 km). The model velocity generally agrees with that of measured up to ~ 0630 UT including the sunward ion flow in the cusp and outbound TBL (Plate B1(b)). In the stagnant MSH decelerated flow still continue the downtail streamline ($V_x < 0$, $V_z > 0$). The impulsive flows at 0400- 0440 UT look to be of the local origin having unpredicted high velocities and strong V_y components: at 0402 UT $\mathbf{V} = (28 \ 105 \ -73)$ km/s with the $|\mathbf{V}| = 131$ km/s i.e. close to the V_A in MSH, the model $\mathbf{V}_m = (32 \ -16 \ -24)$ km/s; at 0408 UT $\mathbf{V} = (80 \ 68 \ -89)$ km/s with the $|\mathbf{V}| = 138$ km/s i.e. again close to the V_A in MSH, the model $\mathbf{V}_m = (32 \ -11 \ -19)$ km/s; and finally at 0436 UT $\mathbf{V} = (100 \ 50 \ -71)$ km/s with the $|\mathbf{V}| = 133$ km/s, the model $\mathbf{V}_m = (4 \ -39 \ -30)$ km/s. We have already discussed above the measured wave trains at 0640- 0710 UT. Here we would like to remind that, while the wavy-velocity jets aren't reproduced by the model, they still might originate from the RRS. However, we assume local origin of the main TBL fluctuations (see

previous section). Indeed, in Plate A4 the thick intensive current sheet spreads from the sunward wall of the outer cusp throat till RRS, i.e. the model infers a stretched-out disturbed zone. We can't check that from the spacecraft data on May 29, 1996 but the model indicates on the probable TBL spread from RRS till the sunward OT wall (i.e. ~ 0430 UT in Plates B1 and B4).

We present in Plate A5 the model plasma density on the $Y=-3.5R_E$ plane and field lines through Interball orbit at 03:14 UT (white) and $\pm 0.25 R_E$ around the central field line (green). The $-3.5 R_E$ plane in the Plate is transparent so that the field lines are brighter when they are in front of the plane and are dimmer when they are behind the plane. The MSH is well depicted by the density maximum between BS and empty magnetosphere. On the closed magnetospheric lines (white and inner green ones) density enhancements are seen sunward these kinked lines (which are mostly out of the semi-transparent density plane). Both the line shapes and location of these cusp-like density maxima indicate on the RRS as the general model source of the MSH plasma inside magnetosphere. The outer from the Earth green field line is the reconnected one, the southern former-MSH part of which is draped over the southern cusp. Thus the model predicts crossing by Interball the reconnected line, originated from the remote reconnection site (at about the same place as the RRS in Plate A4). The model magnetic field satisfactory reproduces the average measured one (Russell et al., 1998). Note the positive/negative model V_x/V_z velocity drift just prior MP in Plate A2(e), the model reproduces the average tendency of the measured speed, but not its fine structure (i.e. the wave train). The most probable reason for that is rather crude model grid ($> 0.2 R_E$, see details in Fedder et al., 1995), while influence of the local medium-scale disturbances, reproduced by the model, on the global structure is not excluded (see discussions above at the beginning of this section). One can see a systematic difference in the measured and model V_x between MP and 0330 UT, after that time V_x well fits the model. Detailed study of high-resolution ion data by Avanov et al. (2001) provides further proofs for the registration of the features predicted by the model reconnection site being downtail Interball (Alfvénic field aligned flows in de Hofmann-Teller frame, stress balance fulfilling etc.).

As we have mentioned in the Introduction, on May 29, 1996 cusp has been sampled from the upper ionosphere till the interface with the MSH. The MHD model serves to link the measurements at different altitudes relative to the RRS, remember the model is adjusted to the SW input. Respective summary picture of the cusp and BL encounters by 5 spacecraft, projected to ionosphere, is depicted in Figure 5 along with the RRS traces and characteristic equipotential patterns from global MHD simulations in the coordinates invariant latitude and MLT in the northern hemisphere. From Figure 5A one can see that the multi-spacecraft data provide the

unprecedented wide coverage of the high latitude magnetic field lines in the invariant latitude, MLT and UT. At lower altitudes the HEO 95-034 and DMSP F12 and F13 registered cusp, shown by the thick blue lines (their traces have been calculated without usage of the MHD model, see Grande *et al.*, 1997 for details). The crosses show projections of the reconnection locations from the global MHD model. Figure 5A demonstrates wide cusp, the TBL (red thick lines) and even mantle (green line) spread in MLT and UT. Figures 5B and 5C show the characteristic ionospheric equipotential patterns from the global MHD model, equipotential contours are plotted for cross-cap potential 6 kV and field-aligned current $4 \cdot 10^{-6}$ A/m. Note, that the ionospheric convection is along the equipotential contours, the convection directions are displayed by the green arrows in the center and by the gray ones at the periphery. Traces of Polar (violet asterisks), Interball-1 (red circled triangle) and reconnection point footprints (brown arrow) are depicted as well. The Figure 5B presents the main features of the MHD model convection till 0306 UT (inclusively). The global MHD model predicts Polar connection to the northern pole for the entire period, while Interball has no such connection starting from \sim 0320 UT, that's why it does not appear in Figure 5C. The latter is in good correspondence with the Interball outbound MP at 0317 UT in Plate A2.

Now we would like to address the problem of the mechanism for the MSH plasma penetration into the cusp. We assume that we have shown and sited enough experimental evidences for the RRS operation being in satisfactory agreement with the MHD model predictions. Now we consider three ways of the cusp populating by the RRS:

- filling while RRS merging ongoing ('merging filling');
- convection inside MP of the filled by merging lines (closed) after merging termination ('convection filling');
- filling through the interconnected in the RRS lines after merging termination ('interconnection filling').

To estimate the trace range of 'merging filling' we take the maximum convection distance for the cusp ions with the measured characteristic energy \sim 500 eV, injected parallel to magnetic field at RRS. For 2 km/s as the reasonable limit of ionospheric convection, one gets the trace drift \sim 200 km (projected on ionosphere) during time-of-flight of parallel 500 eV ions from the RRS to ionosphere. The drift ionospheric velocity of 2 km fits the measured average positive $V_x \leq 50$ km/s in Plate B1(b) at 0400- 0430 UT taking into account scaling factor from the MP to ionosphere. The tracks of ions, traveling back towards the MP, will be shifted \sim 400 km. The isotropic cusp ions at 0130-0220 UT (Plate A2(a)) are seen at \sim 2500 km from the RRS trace. I.e. more than in 5 times larger than the drift path of reflected ions. This is best seen in Figure 5B: the

RRS proves to drive the two-cell sunward (see green arrow in the center) convection with the strong downward component due to large IMF B_y . Returning to the plasma reaching the ionosphere from the RRS while merging lasts, one can see that the plasma from RRS can't account for the Interball-1 cusp at 0130-0220 UT: Interball trace is too far away. Obviously, the same is true for the HEO95-034 and the most of the DMSP cusp periods.

In Figures 5B and 5C one can see that reconnection drives the ionospheric convection (see the arrows), the contours display permanent direction of the ionospheric flows upstream the reconnection site projections throughout several hundreds km. We suppose that it results from narrowness of the RRS flows at its location, the flow direction corresponds to the antiparallel magnetic fields inside and outside the magnetosphere. The latter infers that the kinked reconnected lines are transported towards dayside border of the cusp (after merging termination) in rather narrow angle range. After the second reconnection in the southern hemisphere such over-draped line could become a part of low latitude boundary layer (LLBL, see Onsager et al., 2001 and references therein). Our expectation for the narrow reconnected flows is supported by the fact that in Plate B1(a,b) outside the MP, i.e. during positive B_z , generally $V_x < 0$ (both the measured and model). Thus the majority of the MSH field lines in the decelerated OT moves tailward. Only two thin jets with $V_x > 0$, $V_z < 0$ (i.e. probable flows from RRS) are seen at 0510 and 0618 UT in the measured velocity during stable $B_z > 0$ in the MSH, the first has counterpart in the model one at 0520 UT (with mentioned above 10-minutes shift). We infer from that the narrowness of the sunward RRS flows as compared with the OT width: Polar traced OT through more than $2 R_e$ in X and almost $3 R_e$ in GSM Y directions (see Figure 6), i.e. comparable with the average dimensions of the OT (Savin et al., 1998b). Looking now in Figure 5 we would like to conclude that 'interconnection filling' in the narrow angle range (~ in the green arrow directions) might account for the cusp on HEO at early dawn and noon trace part, on DMSP at 0108 UT and at low latitude at 0250 and small portion of the trace at 0430 UT. We will discuss the interconnected line filling in the 'Discussion and conclusion' section.

As for the 'convection filling', comparison of Figures 5A and 5B, 5C shows that: (a) only ~ half DMSP cusps at high latitudes could be accounted by the convection, (b) Interball cusp at ~ 0209 UT lies on respective convection line but the convection time is ~ 1 hour that seems to be too long (cf. variability of RRS traces in Figure 5A), (c) Polar cusp can originate from the 'convection filling', (d) HEO cusp is inconsistent with it.

We would like to resume, that the dusk cusp on HEO, low latitude DMSP cusp at 0430 UT adjacent to HEO and most probably Interball cusp at ~ 02 UT can't be accounted by the three

processes compatible with the MHD model. The cusp widespread and stability versus quite changeable RMS trace positions in Figure 5A also conform to that (cf. Savin et al., 1998a). So, the combined model and in situ data support the suggestion that the RRS can't be the only major source for the all cusp-like plasma, registered on that day.

5 INTERBALL-1 TBL ENCOUNTERS ON MARCH 1997- 1998

We would like to relate the described case to the similar TBL crossings by Interball-1. From March 1997 - to March 1998 the Interball-1 orbit evolution provided opportunity to cross the near-cusp MP along with the boundary between mantle and LLBL in the near tail twice per orbit (excluding late October - late December period). This orbit is the unique one for spacecraft with plasma and field experiments aboard. For this study we use the routinely calculated dispersion of Bx raw magnetic field waveform with sampling rate 4 Hz at the 20-second intervals (i.e. for 0.05-2 Hz). To fit Df in Plates A2 and B1 we multiply the Bx power variance by factor 3: for the statistical study we accept equality of the ULF power at all 3 magnetic components. We give the AC magnetic pressure ($= Df = \text{RMS}^2$) in [eV/cc] for comparison. For the TBL we have chosen threshold of the maximum root mean square $\text{RMS} > 6 \text{ nT}$ (90 eV/cc) on the 10 minute interval and maximum RMS being higher than the average MSH RMS ($> 150\%$). We display the maximum RMS amplitude in an event in Figure 6. An event is regarded as the continuous one if the RMS exceeds the threshold with interrupts less than 10 minutes. We limit our study outward the magnetosphere by minimum of two values: (a) half a distance between most distant from the Earth MP and closest to the Earth bow shock (BS) at the same orbit, (b) 3 Re outward from the most distant MP. We exclude single RMS spikes clearly corresponded to the main magnetic field jumps at MP. In the selected 1-year period we have identified 150 events near MP. The average value of the RMS maximum equals 15 nT (563 eV/cc), the absolute RMS maximum is over 30 nT (2250 eV/cc). The data gap between the southern events and between the respective southern and northern 'wings' (for Y positive or negative) is mainly due to the MP coverage by the one-year Interball-1 orbit.

There are two features we would like to outline:

- the near-cusp indentation visible in the northern TBL in the XZ and YZ planes; this indentation corresponds to the MP one reported in the OT by Savin et al. (1998b) and Urquhart et

al. (1998). The May 29, 1996 case, displayed in Plates A2 and B1, is namely in this indentation (triangles for Interball-1 and crossed circles for Polar). It is not included in the 1-year statistics.

- the TBL 'wings', ranging from the near-cusp TBL into the tail down to $X \sim -20 R_E$; these 'wings' are in the vicinity of the boundary between semi-open mantle lines and closed LLBL lines, the local minimum in the total magnetic field and currents providing field rotation from the open to closed lines are anticipated there.

The presence of the TBL 'wings' for any IMF direction invokes the MSH plasma penetration not only in the cusp-shaped dayside region, but in the wider one (cf. Haerendel *et al.*, 1978). This is valid in both cases: if turbulent diffusion provides the necessary mass transport and/or if the turbulence serves as the indicator of the local reconnections. Recently Maynard *et al.*, (2001) demonstrated the penetration of the MSH plasma into the tail 'sash' in conjunction with the flank TBL. Note, that although in Klimov *et al.* (1997) and Savin *et al.* (1997) the TBL-like signatures in the tail has been reported, nobody knew if this TBL is present there more or less permanently. For the 'magnetic bubbles' we use for statistics maximum depths of the spiky drops in total magnetic field (Bt). We believe that the Bt drops are accounted by the diamagnetic effect of the heated MSH plasma inside the 'magnetic bubbles'. This agrees both with the Polar data in Plate B1(a,c) and with Interball-1 ones in Savin *et al.* (1998b). The 'bubbles' distribution (not shown) is generally the same as the RMS on in Figure 6. The averaged maximum plasma pressure excess in 'magnetic bubbles' for the March 1997-March 1998 period is $d(NT) = 2160 \text{ eV/cc}$, the absolute maximum of the $d(NT)$ reaches 7000 eV/cc . The magnetic field inside the 'bubble' is in 8,3 times weaker than outside for this year. Taking plasma density in TBL of $5-10 \text{ 1/cc}$, one gets the plasma heating on $216-430 \text{ eV}$ inside the 'magnetic bubbles', i.e. heating in 1.5-3 times relative to the temperature of the MSH ions. This is in good correspondence with speculative predictions of Haerendel (1978). The most events with $RMS > 15 \text{ nT}$ and $d(NT) > 3100 \text{ eV/cc}$ are seen at $|Z| > 4 R_E$, the maximum above the cusp is most prominent. Intensive heating in the high latitude tail 'wings' is seen only till $X = -6 R_E$. As for the low latitudes, there are a number of intensive events e.g. from Geotail data on January 27, 1997 (circles 'G', see next section) and on August 27, 1995 (squared white 'G'), the latter occurred during highly disturbed conditions (see also Figure 1A and related discussions). To compare the level of the ULF magnetic fluctuations near the magnetopause with that of bow shock, we have selected 98 bow shock crossings on the same orbits. The averaged maximum RMS for the bow shock is 1.14 times less than that of TB. In about a half of these 98 cases we have also compared the RMS at the MP and BS for the band of 2-8 Hz (versus 0.05-2 Hz for Figure 6). In this frequency range the characteristic maximum at BS is 2-3

nT, i.e. in 1.5-2 times higher than that in the TBL at the same orbit. It agrees with the few Hz dominant turbulence at the BS (see e.g. Klimov *et al.*, 1997 and references therein), their characteristic amplitude is much less than in the TBL. We should mention, that one cannot exclude that the frequency dependence of the BS-origin waves in the plasma rest frame might fit some characteristic TBL spectra in Figure 1. But to check this one should succeed to subtract correctly the Doppler shift from the near bow shock waves (cf. Romanov *et al.*, 1991).

6 DISCUSSION AND CONCLUSIONS

In this paper we have presented primarily only one case of multi-spacecraft data comparison, i.e., May 29, 1996, but this case demonstrates the general features of the TBL. The uniqueness of the stable and dominant IMF $B_z > 0$ allows us to compare quantitatively the high-shear TBL on Interball-1 (~ 0316 UT) and on Polar (~ 07 UT, cf. Savin *et al.*, 1998b) with the low-shear TBL on Polar (at ~ 04 UT, cf. Romanov *et al.*, 1999) using Interball-1 as the upstream MSH monitor. Here we discuss the achievements of Interball-1 and other contemporary missions in exploration of the MSH-cusp interface on the basis of both the presented above data and of the already published results.

6.1 TBL COMMON PROPERTIES

An inspection of one-year Interball-1 statistics (Figure 6) shows that on May 29, 1996 the TBL as determined by Polar and Interball is closer to the Earth than it is on other days, but this can be explained by an unusually high MSH density (see Figure 4 and Urquhart *et al.*, 1997). In the (XY) plane the TBL trace is observed just near noon as shown in Figure 6. Both case and statistical studies show that the interaction of MSH flows with the high latitude MP is neither smooth nor laminar. The interaction produces a layer with strong non-linear turbulence – the TBL. It is not limited by the near-MP part of the stagnation region over the cusps (see Plate A1), but spreads tailward until X about -15 R_e , maximizing along the transition region from the mantle to the low latitude boundary layer. One-year Interball-1 data show that the TBL is present in 83 % of the

cases (with average amplitude ~ 15 nT). Most TBL-like events are seen at high latitudes, i.e. at $4 < |Z| < 15$ Re. The most intense events could be approximated by the effective disk with diameter of 6 Re above the dayside cusps with an average maximum RMS of about 22 nT (see also Savin et al., 1999). The minor part of TBL-like crossings goes down to the equator; the dynamical interactions seem to dominate there. Examples of Geotail data also show that the turbulence level, both at dayside and low-latitude tail field lines, might be high enough in comparison with the average TBL one over the cusps, especially under disturbed SW conditions. Essential MSH plasma heating (~ 300 eV) occurs in 82 % of the cases within the TBL ‘magnetic bubbles’. The magnetic field in the ‘bubbles’ is highly reduced (8.3 times on average). Some of the magnetic bubbles are transported across the MP (Savin *et al.*, 1998b, 1999, 2002 and Romanov *et al.*, 1999), constituting a mechanism for inward plasma transport. The RMS magnetic field intensity has a tendency to fall tailward in the TBL ‘wings’ that expand into the tail (Figure 6). Intense heating is seen until $X = -6$ Re. The TBL ‘wings’ indicate the possibility of MSH plasma penetration into a wider region than just over the dayside cusps (cf. Haerendel *et al.*, 1978, Savin et al., 1999, Romanov et al., 1999).

6.2 MULTISCALE RECONNECTION

On May 29, 1996, the data display typical TBL features (Plates A2 and B1): wideband intensive magnetic nonlinear fluctuations (with energy density up to 33% of full plasma energy density in flowing MSH), ‘diamagnetic bubbles’ with $|\mathbf{B}|$ drops from ~ 100 nT down to few nT (Figure 4), plasma heating and nearly Alfvénic field-aligned jets etc. (cf. Savin et al., 1998b, 1999, 2002, Sandahl et al., 2000, Stasiewicz et al., 2001, Dubinin et al., 2001). We suggest that the high absolute disturbances during this day can result from the high MSH energy density (~ 15 keV/cc on Polar versus 2-3 keV/cc for average Interball-1 crossings). Both maximum and average Ti growths in the Polar inbound TBL (at ~ 07 UT) are ~ 2 times than those in the low-shear TBL (at ~ 0430 UT). The ion heating (~ 3 times) at ~ 0430 UT in Plate B1 fits the Interball-1 average ion heating profile as shown by the statistics. We attribute this visible difference in the ion heating and doubling of the fluctuation power to the local annihilation of the antiparallel average fields inside/outside the MP. Later in this section we refer to this as ‘primary cusp reconnection’. Its characteristic scale is estimated as 1000-2000 km (see Figure 1A and 2A and related discussions

above). Savin *et al.*, 1998b suggested that such merging might contribute to the TBL energetics along with the smaller scale bursty reconnection of fluctuating fields (of ~ hundreds km). The sunward Alfvénic jets represent direct evidence for the merging (Figure 4). Input from local processes is confirmed by the out-flowing Poynting flux (Plate B2). On the other hand, the wide and long current sheet in Plate A4 upstream of the remote reconnection site (RRS) infers possible continuation of the TBL from the cusp throat to the RRS (Plates A1, A3).

A possible geometry of antiparallel merging in the TBL is depicted in Plate A3. We approximate the MP grid by a smooth function adjusted to the MP crossing positions and respective MP normals (see Savin *et al.* 1998a) with the distance to the subsolar point corresponding to the average SW dynamic pressure from 03 to 07 UT. A comparison of the measured normals with the model of Urquhart *et al.*, 1997 shows that the model does not reproduce the normal inclination towards the noon meridian, which is especially substantial in the case of the Polar outbound at 0409 UT. To determine the qualitative effect of the measured normals on the magnetopause shape we have chosen the disturbance to the average symmetric (relative to X) MP surface (R0, see Urquhart *et al.*, 1997) with the subsolar point at $X = 7.5 R_E$ in the form:

$$R0/R = 1 + 0.24 \exp(-(((L - 60) / 7)((F - 90) / 15))^2) + \\ 0.25 \exp(-(((L - 77) / 15)((F - 88) / 60))^2)$$

where $L = \arccos (X / R0)$, $F = \arctg (ZGSM / YGSM)$ in degrees. The parameters for the disturbance have been chosen from the best fit to the three magnetopause crossings and to reproduction of the normal behaviors. The MP normals are shown by thick blue arrows at the positions of the main MP current sheets (Savin *et al.*, 1998a). At the bottom of Plate A3 we show the normal vector length of $6 R_E$ (i.e., the shorter normal has projection perpendicular to the plate plane). Interball and Polar orbit traces are depicted in Plate A3 by the dashed violet and brown arrows, respectively. The approximate position of the model ‘remote reconnection site’ is marked by the framed ‘RRS’ in Plate A4. The original magnetospheric field lines are marked by green, and those of the IMF by red. The framed ‘Mantle’ stands for the mantle-like ions flowing tailward along field lines at ~ 0230-03 UT in Plate A2(a). A blue grid outlines the average MP indentation. The most intense TBL from Figure 6 is schematically displayed by green dot shadowing. The disturbed wavy reconnected lines are shown near the center of the smooth MP indentation. This reflects the measured nearly antiparallel magnetic fields across the MP at ~ 07 UT in Plate B1 and Figure 4 with the wave-train TBL transition (see also Plates B3- 5). Our comparison of the measured and model data, along with the high-resolution ion data analysis on Interball by Avinov

et al., 2001, support that the model merging (RRS) is located at approximately the predicted location. Certainly, a crude model grid is unable to reproduce the wavy jet fine structure. The antiparallel field situations for very different IMF can be found almost always in the outer cusp throat because of magnetic field elongation over the indented MP by the high-beta MSH flow. At the same time, antiparallel fields are usually seen away from the outer cusp throat at the smooth MP (i.e. in the RRS) also. For northern IMF a case with (at least) two antiparallel merging sites is illustrated in Plate A2. Savin et al. (2001b) presented a similar picture for the southern IMF; the Magion-4 statistics of the sunward flows in the exterior cusp for IMF $B_z < 0$ provide a strong indication of local reconnection.

Fedorov et al., 2000, Dubinin et al., 2001 and Merka et al., 2000 also provided experimental evidence for local penetration of the MSH plasma at high latitudes in the cusp vicinity. Belmont and Rezeau, 2001 developed the linear theory, which predicts that strong ULF fluctuations that occur just outside of or at the magnetopause can independently result in micro-reconnection and local plasma penetration all along the magnetopause surface even in the absence of quasi-stationary macro-reconnection of antiparallel magnetic fields. In our presentation we outlined highly deflected (especially in the Y direction, see Plate B1(b) and comparison with the model above), almost Alfvénic flows in the outbound TBL at about 0430 UT for quasi-parallel magnetic fields at the MP. Because annihilation of the average field is not possible there, we attribute these features to the by-product reconnection of the fluctuating fields in the TBL. Another possibility is that secondary reconnection of the fluctuating fields in the TBL (regardless of the origin of the TBL) can provide the plasma inflow in the quasi-parallel case. This reasoning is along the lines of the Haerendel (1978) predictions and findings of Savin *et al.*, 1998b for other IMF directions. The reconnection bursts can provide a particular mechanism for the effective ‘interconnection of the parallel fields’ (see Chandler *et al.*, 1999 and references therein). On the other hand, the micro-reconnection creates the specific structure of the MP current sheet(s) with magnetic islands, which results in plasma percolation through the non-linear boundary network (Kuznetsova and Zelenyi, 1990). The order-of-magnitude estimate shows that this stochastic plasma transfer through the TBL/cusp walls might provide a means of populating both the cusp and low latitude boundary layer (LLBL): the diffusion coefficient $D_p \sim (5-10) 10^9 \text{ m}^2/\text{s}$ for typical MP parameters results in a particle influx of $(1-2) 10^{27}$ particles /s (Savin et al., 1999). Primary cusp reconnection should certainly amplify the plasma inflow. Summarizing the discussion above, on May 29, 1996 multiple reconnection sites might operate simultaneously:

- Remote (from the cusp) reconnection site (RRS) that is predicted by the MHD model (Fedder *et al.*, 1995) and the scale of which can be evaluated up to a few earth radii;
- Primary cusp reconnection site(s) at the location of the antiparallel average fields (of ~ few thousand km), where local magnetic field annihilation enforces the fluctuation level and heating;
- Secondary reconnections of the highly fluctuating fields potentially at all locations within the TBL, that can occur at small scales (down to an ion gyroradius) even for the low-shear average fields (cf. Haerendel 1978, Savin *et al.*, 1998b and Chandler *et al.*, 1999).

In Plate A3 these three types of reconnection are shown schematically by laminar reconnected lines marked 'RRS', wavy reconnected lines in the TBL and green dot shadowing, respectively.

6.3 LOCAL VERSUS REMOTE MECHANISMS OF MSH PLASMA PENETRATION INTO CUSPS

Despite the problem of MSH plasma penetration being far from its final solution, we would like to discuss the experimental evidence for the operation of local cusp processes.

The cusp at different altitudes and latitudes as observed by Polar, Interball-1, HEO 95-034, and DMSP F13 and F13 seems to be rather far from field lines of the RRS traces (Figure 5). As we have mentioned above, the cusp can hardly be populated by the MSH plasma, which enters the MP on the tail field lines only. Local penetration by the MSH plasma on the dayside field lines should be involved, e.g. at 04 UT in Plate B1 and in the dusk cusp on HEO in Figure 5 (see related discussion above, cf. 'entry layer' by Paschmann *et al.*, 1976). Savin *et al.* (1998a) have pointed out that the observation of the TBL at three points in the range 0830 - 1500 MLT and $57 - 67^\circ$ of geomagnetic latitude over a period of 4 hours is a strong argument for a temporally-persistent existence of this TBL (see also Figure 5). As the RRS trace moves in the range 16-01 MLT and $80-90^\circ$, the stable TBL seems to be a more appropriate widespread source for the cusp on May 29, 1996. The MHD model depicts the access of the upstream MSH flows deep inside the outer cusp throat (dominated by $V_x < 0$ in Plate B1(b), see discussion above). Similar to the cases with IMF $B_z < 0$ from Savin *et al.* (1998b), these flows interact with the tailward outer cusp throat. On the other hand the sunward flows with reconnected kinked field lines are predicted and actually observed but only in very narrow regions over the OT. Thus we assume that, although this remote

reconnection process operates, its relative importance might be small in comparison with the permanently operating TBL primary and secondary mergings.

Onsager et al. (2001) provided arguments from the electron HYDRA data that at 04:08- 04:20 UT Polar has generally been on the double-reconnected field lines outside the MP (see their Figure 4) that should be a consequence of the large-scale RRS. However, at this time the ions, moving along the magnetic field lines, are the same as in the MSH (excluding the short period of negative magnetospheric-like B_z) while the antiparallel ions are mostly heated (presumably in the MP current layer). The latter infers connection to the northern cusp through the MP (TBL). For the double-reconnected lines the same antiparallel heated ions should be seen at least after the time-of-flight period. For characteristic ion energy ~ 1 keV the time-of-flight is ~ 6 minutes, i.e. two times shorter than the time interval 04:08- 04:20 UT. In this situation we would like to account for electron heating in the parallel and antiparallel directions in the TBL by positioning Polar inside the distributed region of electron acceleration. In fact, the bi-directional electron flows can be seen in different configurations:

- on the closed (at least for electrons) field lines, i.e. namely what Onsager et al. (2001) assumed;
- on the line that connects the ionosphere at one end and touches the electron acceleration region at the other end. For such a configuration the accelerated electrons should be reflected from the convergent part of the field line near the ionosphere in a few seconds and for a stable heating source constitute the bi-directional parallel-heated distribution (cf. Savin et al., 1998b);
- when the electron heating source is distributed or multiple, i.e. seen from both parallel and antiparallel field directions.

To distinguish the spacecraft located at the closed field lines or inside the regions of electron acceleration we compare the electron distributions from Onsager et al. (2001) with wave data shown in Plate B1(f-i). Savin et al. (1997, 1998b) demonstrated that intense waves near the lower hybrid frequency (i.e. \sim several Hz in the TBL) can accelerate electrons along field lines up to the measured energies. Plate B1(f-i) clearly demonstrates that at 0408-0420 UT strong wideband waves are seen up to the electron cyclotron frequency. Panels f and h especially display waves at 5-20 Hz. Thus, the wave data support that electrons in the TBL can be accelerated by the intense ULF waves. It seems that outside the TBL the field topology tracing by electrons could be applied successfully, while distinguishing between options 1 and 2 still remains to be done.

In the TBL on Polar $T_i = 400 - 600$ eV at 0320-0425 UT (see Figure 5A and Plate B1(d)), which are close to pre-noon ion energies measured on HEO at 0135-0315 UT (see Figure 2 in Grande et al., 1997) and to those in the cusp on Interball at 0135 UT (Plate A2(a)). The Polar TBL at 0650

UT with T_i up to 900 eV seems to be an appropriate source for the afternoon mid-altitude cusp on HEO with the average ion energy also ~ 900 eV. These data provide further evidence that in the mid-altitude cusp the MSH plasma supply can be controlled by the local acceleration/heating processes in the respective TBL over the cusp.

We would like to outline further possible consequences of the permanent TBL presence over the cusps. The intense plasma mixing in the TBL can effectively supply ions to the inter-connected flux tube portions, which are close to the MP from the MSH side (cf. 'eddy convection' of Haerendel, 1978, see also Figure 2 and related discussions). This should enforce effective MSH plasma inflow through the inter-connected field lines after the termination of merging (cf. Fedorov et al., 2000). The MP current sheet presumably reflects the electrons and lower energy ions, which have their gyroradii smaller than the sheet/kink characteristic scale (cf. Savin et al., 1998b).

6.4 INTERACTION OF MSH FLOWS WITH THE OUTER CUSP THROAT

Now we would like to address another primary mechanism for the energy and mass transfer at the MSH/cusp interface: the direct interaction of the MSH flow with the outer cusp throat (OT). From Figure 6 and Plates A1, A3, and A4 we see that the MP indentation might present a substantial obstacle for the plasma flow streaming around the MP.

The supersonic flow burst just outside the MP (see Plate A2) can be suggestive of a cusp 'Laval nozzle' according to the theory of Yamauchi and Lundin (1997). However, we believe that the 'rising flank of the tail lobe' presents an obstacle to the MSH flow in the vicinity of the magnetopause (Paschmann et al., 1976), or, in other words, it represents an 'almost vertical outer cusp throat tailward wall' (Savin et al., 1998b). The obstacle slows down and diverts the magnetosheath flow, so that the turbulent boundary layer originates in the stagnation region in front of the obstacle and in its wake (Haerendel, 1978). Yamauchi and Lundin (1997) proposed that the ionospheric ion outflow is the reason for the MSH flow velocity jumping back to a subsonic value. While Polar registered oxygen and He^+ outflow in the outer cusp and TBL (Grande et al., 1997), we suppose that this plasma loading is not the primary cause: the ionospheric particles have negligible contribution to the average mass and energy densities, while both the DC magnetic field pressure (E_m) at the OT wall and in the TBL spikes reach the magnitude of the ion energy density, E_s , in the MSH (see Plates A2(d), B1(c) and Savin et al., 1998a

&b). Both the outer cusp throat and TBL are permanent features of the high latitude magnetopause. Savin et al. (1998a) suggested that the rotational discontinuity (Plate A2(b,d) and Insert A) separates the reconnected and entirely magnetosheath field lines, which agrees with $\mathbf{B}^2/8\pi$ dominating in this region. In the latter case the RD could represent the outer wall for the 'Laval nozzle' that seems to add an element, which has not been specified yet, to the model of Yamauchi and Lundin. Figure 1 in Savin et al., (1998a) displays an IMF discontinuity ~ at the time of the RD. However, as IMF B_y changes in the opposite sense to that observed on Interball, we suppose that the SW parameters changed through the discontinuity, and in turn caused the RD displacement earthward.

Multi-point data on January 27, 1997 (Savin et al., 1998c) provide an opportunity to get the quantitative estimate for the drop of the kinetic energy density, E_k (relative to the thermal one, E_t) due to the MSH flow interactions with the tailward cusp wall. The model of Spreiter and Stahara, 1980 predicts the gain of E_k/E_t to be ~ 2 for Geotail relative to Interball-1 in Figure 2 of Savin et al. (1998c) at ~ 1120 UT, while the measured gain is ~ 8 , i.e., E_k/E_t drops by a factor of ~ 4 at high latitudes in comparison to the simultaneously obtained low latitude values at the same X.

Following Haerendel 1978 we address this deceleration to the MSH flow interaction with rising field lines at the tailward wall of the outer cusp throat. The sound Mach number in the unperturbed MSH ($M_s \sim 2.1$) drops to $M_s < 1$ downstream of the cusp obstacle on April 21 1996 (Savin *et al.*, 1998b). $M_s \sim 2$ is also seen in the Interball-1 data just outside the MP (Plate A2), while the flow/discontinuity geometry in the cusp throat is not clear enough yet. The M_s supersonic/subsonic transitions are compatible with the existence of slow/intermediate shocks (see e.g. Russell 1995 and references therein) in the vicinity of the tailward cusp wall (cf. Yamauchi and Lundin, 1997 and Savin *et al.*, 1998b). Thus, we think that the finding of the MSH flow deceleration/heating downstream of the high latitude cusp represents a valuable result from the multi-spacecraft IACG Campaign #2 that outlines the significance of the bulk flow energy transformation in the process of the flow interaction with the outer cusp throat.

For the comparison of transient events at high and low altitudes, ion back-tracing should be modified to include scattering and reflection of ion flows in the TBL. We would like to point out also that the TBL not only regulates the penetration of the 'remote' (e.g. from RRS) ion flows, but also provides both plasma penetration from the MSH and secondary magnetic flux reconnection. This magnetic flux, reconnected at small scales, on average, is capable of driving magnetospheric convection (Haerendel, 1978). In fact at this point we touch an open critical problem of the SW/magnetosphere interaction: where are the Earth magnetic field lines being opened? Our

current understanding is that this process is one of multi-point and multi-scale. We believe that the MSH/cusp interface plays the dominant role at least in quasi-steady conditions.

The tilt angle dependence of the cusp position both at high and low altitudes (Zhou *et al.*, 1999, Merka *et al.*, 1998, Smith and Lockwood, 1996) has a natural explanation if the TBL is a general source of plasma for the cusps:

(a) the higher the tilt (i.e. the closer the dipole axis to the Sun), the more open the OT for the external MSH flow (i.e. the OT tailward wall represents the steeper obstacle for the MSH flow); (b) the higher the shift/penetrations at the OT tailward wall, the deeper the MSH plasma will be seen on the tail field lines; (c) the deeper the plasma penetration (and/or tailward field line deflection), the more tailward it will be projected into the polar cap (i.e. the cusp is at higher invariant latitudes). Note that the tilt-related cusp shift has no explanation in the ‘traditional’ global-reconnection approach.

6.5 TBL SOURCES AND CHARACTER

Following Haerendel (1978), we suppose that first of all the TBL results from the turbulent mixing driven by the regular MSH flow interaction with the deformed near-cusp magnetopause. The disturbed flows, accelerated in the remote reconnection site, can contribute to the TBL generation as well. Remote reconnection site also regulates the TBL position by shifting the MP indentation according to the SW parameters. Away from the plasma stagnation region in the OT center, the Kelvin-Helmholtz plasma vortices with secondary reconnections should provide a mechanism for plasma heating/transport (cf. Chen *et al.*, 1998). The fluctuation level in the MSH, especially downstream of quasi-parallel bow shocks, is believed to stimulate the ULF turbulence generation in the TBL. In some cases mentioned above, the correlation at the time interval of ~ 5-15 minutes in the post-BS region and middle MSH and in the OT reaches 0.6- 0.7 and is a manifestation of the TBL/MP reactions to the SW/MSH transients. Thus, the transient current sheets and density gradients generated by dynamic SW interactions with the MP should contribute in the TBL energy balance. We think that, as a whole, the TBL collects, transforms and generates the plasma flow and magnetic field disturbances simultaneously from several sources. Its status depends on the short-term time history of the SW/magnetosphere interactions, influencing, in turn, the interaction of the magnetosphere with newly-arriving disturbances at each particular moment.

Besides the transient/dynamic reactions of the TBL to external disturbances, the TBL appears to have well-defined inherent properties, which we have been fortunate to trace at different points of the MSH and MP boundary layers during the favorable period of relatively steady SW parameters. The modern wavelet technique provides us with strong evidence that the spectral characteristics of the TBL on May 29, 1996 are very well defined. The simultaneous Interball/Polar magnetic data demonstrate the presence of a maximum at 1- 2 mHz throughout the MSH, TBL and inside MP (Figure 1B). The amplification and frequency shift to higher values in the OT might be a local TBL feature (cf. Figure 4 in Savin et al., 2002). Taking the Alfvén speed in the MSH as a proxy for the phase velocity we get 8-15 Re as the characteristic scale, i.e. \sim the size of the dayside MSH or cusp field lines. Such long waves can pass through the MP (see Plate B3) and might resonate with the dayside flux tubes in the PC 4-5 range or at higher harmonics (cf. Pilipenko *et al.*, 1999). The most pronounced TBL waves at 0.005-0.5 Hz have the characteristic kinked shapes and slopes (Figure 1B). The spectral power here is much higher than that of fluctuations in the flowing and stagnant MSH and the spectral shape is also different. We have checked the waves in the TBL on August 26, 1995, June 19 and 23, 1998 and found that the kinked shape with slopes of 1-1.5 and 2-2.6 are characteristic for the TBL. Spectral peaks at lower frequencies might also appear. A substantial TBL feature, which we think occasionally coincides with a simultaneous one in the MSH in Figure 1B, is the frequency of the kink (cf. asterisks and crosses). Thus, the characteristic time/space scale, which corresponds to the kink, might be thought to originate uniquely in the MSH. However, the Polar data just over the TBL at 05:00- 05:45 UT show practically no kink and thus do not confirm this suggestion. We would like to attribute the kinked MSH spectra on Interball at 04:08- 04:39 UT e.g. to effects of MSH disturbances, such as intermediate/slow shocks detached from the MP (cf. Russell, 1995), rather than regard them as a common MSH property. The higher value of the slope in the TBL of ~ 2 is close to that characteristic for the developed self-consistent kinetic turbulence in the geomagnetic tail (see e.g. Zelenyi and Milovanov, 1998 and references therein).

Cascade-like wavelet and bicoherence spectrograms and wavelet correlation time infer coherent, most probably three-wave, interaction between wave trains, while the disturbances seem to be random in the waveforms (Figures 3-4 and Plates B3-B6). The local wave trains originate from the interaction of the disturbed MSH flows with the MP. Their dispersion is indicative of kinetic Alfvén waves (KAW, see Figure 1A). Johnson and Cheng (1997) proposed excitation of transverse KAW at the MP by interaction of the compressible MSH waves with the current sheet. Later Belmont and Rezeau (2001) demonstrated the growth of the trapped large-amplitude KAW

inside the non-uniform current sheets. At the nonlinear stage the Alfvénic disturbances in the TBL modulate the incident MSH flow in a self-consistent manner, being globally synchronized by phase coupling with the large-scale variations (at ~ 3 mHz, see Plate B3- B6). While linear KAW resonances (i.e. singularities in the equations of Belmont and Rezeau, 2001) are absent, we suggest that the coherent large-scale structures can originate from the inverse KAW cascades (cf. Plates B3, B5, B6 and Figure 3B). Thus, the chain is closed: the TBL seems to be multi-scale self-organized system of interacting nonlinear waves. This infers qualitative difference from the traditional approach wherein the MSH/cusp interaction is regarded as a linear superposition of magnetospheric responses on the solar wind or MSH disturbances. Note also that the long-term correlation is suggestive of systems out of equilibrium near the critical point (cf. Consolini and Lui, 2000). The kinked TBL spectra with characteristic slopes remarkably resemble those in the near-Earth neutral sheet in the state of the self-organized criticality (see e.g. Zelenyi and Milovanov, 1998).

6.6 CONCLUDING REMARKS

The results of our data analysis strongly indicate that the TBL fluctuations, instead of being random, are highly correlated and organized by the cascades of nonlinear interactions. The selected coherent wave trains are capable of synchronizing interactions throughout the TBL, somewhat resembling a global TBL resonance. Multiplying the characteristic period of the ‘organizing’ wave mode by the MSH Alfvén speed we get 3-4 R_E as a proxy for the characteristic scale. This is close to the diameter of the TBL or outer cusp throat (Plates A1-2) and can be attributed to a standing nonlinear wave, trapped in the outer cusp throat.

We suggest that multi-scale TBL processes play at least a comparable role to those of reconnection remote from the cusp in the solar wind energy transformation and population of the magnetosphere by the MSH plasma.

Acknowledgments. We would like to memorize one of the pioneer in space researches – Professor Y. I. Galperin – the discussions with whom inspired many ideas for this and related papers. We appreciate N. Maynard for providing Polar electric field data, very prominent discussions and help in the preparation of the paper. We thank K. W. Ogilvie and the SWE team for providing WIND

solar wind dynamic pressure data, R. Lepping and J. H. King for providing WIND and Imp-8 magnetic field data, K. Tsuruda for getting available Geotail electric field raw waveform data, W. Peterson for help in getting the POLAR/TIMAS data and J. Scudder for providing the HYDRA data and helpful discussions. We thank the GEOTAIL/MGF team, especially Dr. H. Matsui, for providing their high-resolution magnetic field data used in this paper. We appreciate fruitful discussions with G. Haerendel, A. Fedorov, G. Zimbardo, M. Yamauchi, A. Otto, T. E. Moore, T. G. Onsager and R. Lundin along with the help in the paper preparation by A. B. Belikova, I. Dobrovolsky, K. Sigsbee and V. Prokhorenko. Work was partially supported by International Space Science Institution, and by grants INTAS/ESA 99-1006, INTAS-2000-465, EST.CLG 975277, KBN 8T12E 047 21, RFFR 02-02-17160 and by Humbolt Foundation.

References

- Anderson, R. R., C. C. Harvey, M. M. Hoppe, B. T. Tsurutani, B. T. Eastman, J. Etcheto**, Plasma waves near the magnetopause, *J. Geophys. Res.*, **87**, 2087, (1982).
- Angelopoulos, V., F.S. Mozer, J; Bonnell, M. Temerin, M. Somoza, W.K. Peterson, H.L. Collin, and B. Giles**, Wave power studies of cusp crossings with the Polar satellite, *J. Geophys. Res.*, 106(A4), 5987, (2001)
- Avanov, L.A., V. N. Smirnov, J. H. Waite, Jr., S. A. Fuselier, and O. L. Vaisberg**, High-latitude magnetic reconnection in sub-alfvénic flow: Interball Tail observations on 29 May 1996, *J. Geophys. Res.*, **106**, submitted (2001)
- Belmont, G. and L. Rezeau**, Magnetopause reconnection induced by Hall-MHD fluctuations, *J. Geophys. Res.*, **106** (A6), 10,751-10,760, (2001)
- Belova, E. V., J. Blecki, M. Denis, L. M. Zelenyi, and S. P. Savin**, Excitation of ion cyclotron waves at the boundary of the magnetosphere, *Sov. J. Plasma Phys.*, **17**, 555, (1991)
- Blecki, J., H. Rothkaehl, K. Kossacki et al.**, ULF-ELF-VLF-HF Plasma Wave Observations in the Polar Cusp Onboard High and Low Altitude Satellites, *Phys. Scripta*, **75**, pp. 259-263, (1998)
- Chandler, M. O., S. A. Fuselier, M. Lockwood, and T. E. Moore**, Evidence of component merging equatorward of the cusp, *J. Geophys. Res.*, **104**, 22,623, (1999).
- Chen, S.-H., S. A. Boardsen, S. F. Fung, J. L. Green, R. L. Kessel, L. C. Tan, T. E. Eastman, and J. D. Craven**, Exterior and interior polar cusps: Observations from Hawkeye, *J. Geophys. Res.*, **102**(A6), p. 11335, (1997)
- Chen, Q., A. Otto, L. C. Lee**, Tearing instability, Kelvin-Helmholtz Instability and Magnetic Reconnection, *J. Geophys. Res.*, **102** (A1), p. 151, (1997)
- Consolini, G. and A. T. Lui**, Symmetry breaking and nonlinear wave-wave interaction in current disruption: possible evidence for a phase transition, in *Magnetospheric Current Systems*, Geophysical Monograph **118**, American Geophysical Union, Washington D.C., pp. 395-401, (2000)
- Dubinin, E., A. Skalsky, P. Song, S. Savin, J. Kozyra, T. E. Moore, C. T. Russell, M. O. Chandler, A. Fedorov, L. Avanov, J. A. Sauvaud, R. H. W. Friedel**, Polar-Interball coordinated observations of plasma characteristics in the region of the northern and southern distant cusps, *J. Geophys. Res.*, **107**, A5, 10.1029/2001JA900068, (2002)
- Dungey, J. W.**, The structure of the exosphere, or adventure in velocity space in *Geophysics the Earth's Environment*, edited by C. DeWitt, J. Hieblot and A. Lebeau p.505, *Gordon and Breach*, New York, (1963)

- Fedder, J. A., J. G. Lyon, C. M. Mobarry, and S. P. Slinker**, Topological structure of the magnetotail as a function of interplanetary magnetic field direction, in *J. Geophys. Res.*, **100**, 3613, (1995)
- Fedorov, A., E. Dubinin, P. Song, E. Budnick, P. Larson, J.A. Sauvaud**, Characteristics of the exterior cusp for steady southward IMF: Interball observations, *J. Geophys. Res.*, **105**, 15,945- 15,957, (2000).
- Fung, S. F., T. E. Eastman, S. A. Boardsen and S.-H. Chen**, High-altitude cusp positions sampled by the Hawkeye satellite, *Phys. Chem. Earth*, **22**, pp. 653-662 (1997)
- Grande, M., J. Fennell, S. Livi, et al**, Observations of the mid-Altitude Magnetosheath During a Persistent Northward IMF Condition: Polar CAMMICE Observations, *Geophys. Res. Lett.*, **24**, pp. 1475-1478 (1997)
- Haerendel, G. and G. Paschmann**, Entry of solar wind plasma into the magnetosphere, in *Physics of the Hot Plasma in the Magnetosphere*, edited by B. Hultqvist and L. Stenflo, p. 23, Plenum, NY, (1975)
- Haerendel, G.**, Microscopic plasma processes related to reconnection, *J. Atmos. Terr. Phys.*, **40**, pp. 343-353 (1978)
- Haerendel, G., et al.**, The frontside boundary layer of the magnetopause and the problem of reconnection, *J. Geophys. Res.*, **83**, 3195, (1978)
- Johnson, J.R., C.Z. Cheng**, Kinetic Alfvén waves and plasma transport at the magnetopause, *Geophys. Res. Lett.*, **24**, p. 1423 (1997)
- Klimov, S. I. et al.**, Investigation of plasma waves by combined wave diagnostic device BUDWAR PROGNOZ-10-INTERCOSMOS, *Cosmic Research (Transl. from Russian)*, **24**, 177, (1986)
- Klimov, S. et al.**, ASPI Experiment: Measurements of Fields and Waves Onboard the INTERBALL-1 Spacecraft, *Ann. Geophys.*, **15**, pp.514-527, (1997)
- Kuznetsova, M. M., and L. M. Zelenyi**, The theory of FTE: Stochastic percolation model, in *Physics of Magnetic Flux Ropes*, edited by C. T. Russell, E. R. Priest, L.C. Lee, pp.473-488, *American Geophysical Union* (1990)
- La Belle-Hamer, A.L., A. Otto, L.C. Lee**, Magnetic reconnection in the presence of sheared flow and density asymmetry: application to the Earth's magnetopause, *J. Geophys. Res.*, **100**, pp. 11,875- 11,889, (1995)
- Lundin, R., J. Woch and M. Yamauchi**, The present understanding of the cusp, in Proceedings of the Cusp Workshop, European Space Agency, *Spec. Publ.*, ESA SP-330, pp.83-95, (1991).
- Maynard, N.C., S.Savin, G.A.Erickson, H.Kawano, Z.Nemecek et al.**, Observation of the magnetospheric "sash" and its implications relative to solar-wind/magnetospheric coupling: A multisatellite event analysis, *J. Geophys. Res.*, **106**, 6097, (2001)
- Merka, J, J. Safrankova, Z. Nemecek, A. Fedorov, N. Borodkova, S. Savin, A. Skalsky**, HIGH ALTITUDE CUSP: INTERBALL OBSERVATIONS, *Adv. Space Res.*, **25**, No. 7/8, pp. 1425-1434, (2000)
- Ogilvie, K. W. et al.**, A comprehensive plasma instrument for the WIND spacecraft, in The Global Geospace Mission, *Space Science Rev.*, **71**, pp. 55-77, (1995)
- Onsager, T.G., J. Scudder, M. Lockwood, C.T. Russell**, Reconnection at the high latitude magnetopause during northward IMF conditions, *J. Geophys. Res.*, in press (2001)
- Paschmann, G., G. Haerendel, N. Sckopke, H. Rosenbauer and P. C. Hedgecock**, Plasma and magnetic field characteristics of the distant polar cusp near local noon: The entry layer, *J. Geophys. Res.*, **81**, 2883, (1976)
- Petrinec, S. M. and C. T. Russell**, An examination of the effect of dipole tilt angle and cusp regions on the shape of the dayside magnetopause, *J. Geophys. Res.*, **100**, pp. 9559-9566, 1995.
- Pilipenko, V., E. Fedorov, N. Mazur, M.J. Engebretson, W.J. Hughes**, Magnetohydrodynamic waveguide/resonator for Pc3 ULF pulsations at cusp latitudes, *Earth Planets Space*, **51**, pp. 441-448 (1999)
- Pottelette, R., M., Malingre, N., Dulouloz, B., Aparicio, et al.**, High frequency waves in the cusp/cleft regions, in *J. Geophys. Res.*, **95**, 5957, 1990.
- Romanov, S. A., S. I. Klimov, P. A. Mironenko**, Experimental Derivation of ELF Wave Dispersion Relations and Evidence of Wave Coupling in the Earth Bow Shock Foot from the Data of the PROGNOZ-10, *Adv. Space Res.* **11**, 19 (1991)

- Romanov, S. A.**, A Correlation Analysis of Vector Variables as Applied to the Study of ELF Interplanetary Plasma Waves, *Cosmic Research*, **36**, No. 4, pp. 339-354 (1998)
- Romanov, V., S.Savin, S.Klimov, S.Romanov, Yu.Yermolaev, J.Bleeki, R.Wronowski**, Magnetic turbulence at the magnetopause: plasma penetration, *J. Tech. Phys. (Poland)*, **40**, 1, 329-332, (1999).
- Russell, C. T.**, The configuration of the magnetosphere, in *Critical Problems of Magnetospheric Physics*, edited by E. R. Dyer, 1-16, *IUCSTP Secretariat*, Washington, D.C., (1972)
- Russell, C. T.**, The structure of the magnetopause, in *Physics of the Magnetopause*, edited by P. Song, B. U. O. Sonnerup and M. F. Thomsen, pp.81-98, *American Geophysical Union* (1995)
- Russell, C. T., *et al.*, The GGS Polar magnetic fields investigation, *Space Sci. Res.*, **21**, pp. 563-582, (1995)
- Russell, C. T.**, *et al.*, Entry of the POLAR spacecraft into the polar cusp under northward IMF conditions, in *Geophys. Res. Lett.*, **25**, 3015 (1998)
- Safrankova, J., Z. Nemecek, D. Sibeck, L. Prech, J. Merka, O. Santolik**, Two-point observation of high-latitude reconnection, *Geophys Res. Lett.*, **25**, pp. 4301-4304, 1998.
- Sandahl, I., B Popielavska, E. Yu. Budnick, A. Fedorov, S. Savin, J. Safrankova, Z. Nemecek**, THE CUSP AS SEEN FROM INTERBALL, Proceedings of 'Cluster II Workshop. Multiscale/Multipoint Plasma Measurements., Imperial College, London, Sept. 22-24, 1999, ESA/ SP-499, p. 39-45, (2000)
- Savin, S. P., O. Balan, N. Borodkova, E. Budnik, N. Nikolaeva, V. Prokhorenko, T. Pulkkinen, et. al.**, Interball Magnetotail Boundary Case Studies, *Adv. Space Res.*, **19**, 993, (1997)
- Savin, S. P.**, ELF waves near the high latitude magnetopause, in *Abstracts of AGU Chapman Conference on Physics of the Magnetopause*, March 14-18, 41, (1994)
- Savin, S. P., S. A. Romanov, A. O. Fedorov, L. Zelenyi, S. I. Klimov, et al.**, The cusp/magnetosheath interface on May 29, 1996: Integball-1 and Polar observations, *Geoph. Res.Lett.*, **25**, pp. 2963-2966, (1998a)
- Savin, S. P., N. L. Borodkova, E. Yu. Budnik, A. O. Fedorov, S. I. Klimov, et al.**, Interball tail probe measurements in outer cusp and boundary layers, in *Geospace Mass and Energy Flow: Results from the International Solar-Terrestrial Physics Program*, edited by J.L. Horwitz, D.L. Gallagher and W.K. Peterson, Geophysical Monograph **104**, American Geophysical Union, Washington D.C., pp. 25-44, (1998b)
- Savin, S., L. Zelenyi, L. Budnik, N. Borodkova, A. Fedorov, et. al.** Manifestations of Boundary Layer Dynamics in Substorm Activity. Multi Spacecraft Study, in *SUBSTORM-4, International Conference on Substorms-4', Lake Hamana, Japan: March 9-13, 1998*, ed. by S. Kokubun and Y. Kamide, pp. 125-130, Terra Scientific Publ. Co., Tokyo, (1998c)
- Savin, S., E. Budnik, M. Nozdrachev, V. Romanov et al.**, On the plasma turbulence ant at the polar cusp outer border, *Czechoslovak J. Phys.*, **49**, 4a, 679-693, (1999)
- Savin S.P., L.M. Zelenyi, S.A. Romanov, S.I. Klimov, A.A. Skalsky et al.**, Tubulent Boundary layer at the Border of Geomagnetic Trap, *JETP Letters*, **74**, No 11, pp. 547- 551, (2001)
- Savin, S., L. Zelenyi, N. Maynard, I. Sandahl, H. Kawano, C. T. Russell et al.**, Multi-spacecraft Tracing of Turbulent Boundary Layer, *Adv. Space Res.*, **30**, No. 12, 2821-2830, (2002a)
- Savin S., J. Buechner, G. Consolini, B. Nikutowski, L. Zelenyi, E. Amata, et al.**, On the properties of turbulent boundary layer over polar cusps, *Nonlinear Processes in Geophysics*, **9**, 443-451, (2002b)
- Sibeck, D. G., R. E. Lopez, E. C. Roelof.**, Solar wind control of the magnetopause shape, location and motion. *J. Geophys. Res.*, **96**, pp. 5489-5495, (1991)
- Smith, M. F., and M. Lockwood**, Earth's magnetospheric cusps, *Rev. of Geophys.*, **34**, 233,(1996)
- Spreiter, J. R., S. S. Stahara.**, A new predictive model for determining solar wind- terrestrial planet interactions, *J. Geophys. Res.*, **85**, pp. 6769-6777, (1980).
- Spreiter, J. R., B. R. Briggs**, Theoretical determination of the form of the boundary of the solar corpuscular stream produced by interaction with the magnetic dipole field of the Earth, *J. Geophys. Res.*, **67**, pp. 37-51, (1962)

- Stasiewicz, K., C. E. Seyler,, G. Gustafsson,, J. Pickett and B. Popielawska**, Magnetic Bubbles and Kinetic Alfven Waves in the High-Latitude Magnetopause Boundary; *J. Geophys. Res.*, **106**, submitted (2001)
- Treumann, R.A., J. Labelle, T.M. Bauer**, Diffusion processes: an observational perspective, in *Physics of the magnetopause*, ed. by P. Song, B.U.O. Sonnerup, M. F. Thomsen, p. 331, American Geophysical Union (1995).
- Urquhart, A. L et al.** , Magnetic field models for Polar magnetopause crossings of May 29, 1996, *J. Geophys. Res.*, **103**, pp. 17,323-17,332, (1998)
- Yamauchi, M., and R. Lundin**, The Wave-Assisted Cups Model: Comparison to Low-Latitude Observations, *Phys. Chem. Earth*, **22**, pp. 729-734, (1997)
- Zelenyi, L.M., A.V. Milovanov**, Multiscale magnetic structure of the distant tail: self-consistent fractal approach, in *New Perspectives on the Earth Magnetotail*, Geophysical Monograph **105**, AGU, Washington D.C., pp. 321-338, (1998)
- Zhou, X.-W. and C. T. Russell**, The location of the high latitude polar cusp and the shape of the surrounding magnetopause, *J. Geophys. Res.*, **102**, pp. 105-110, (1997)

FIGURES

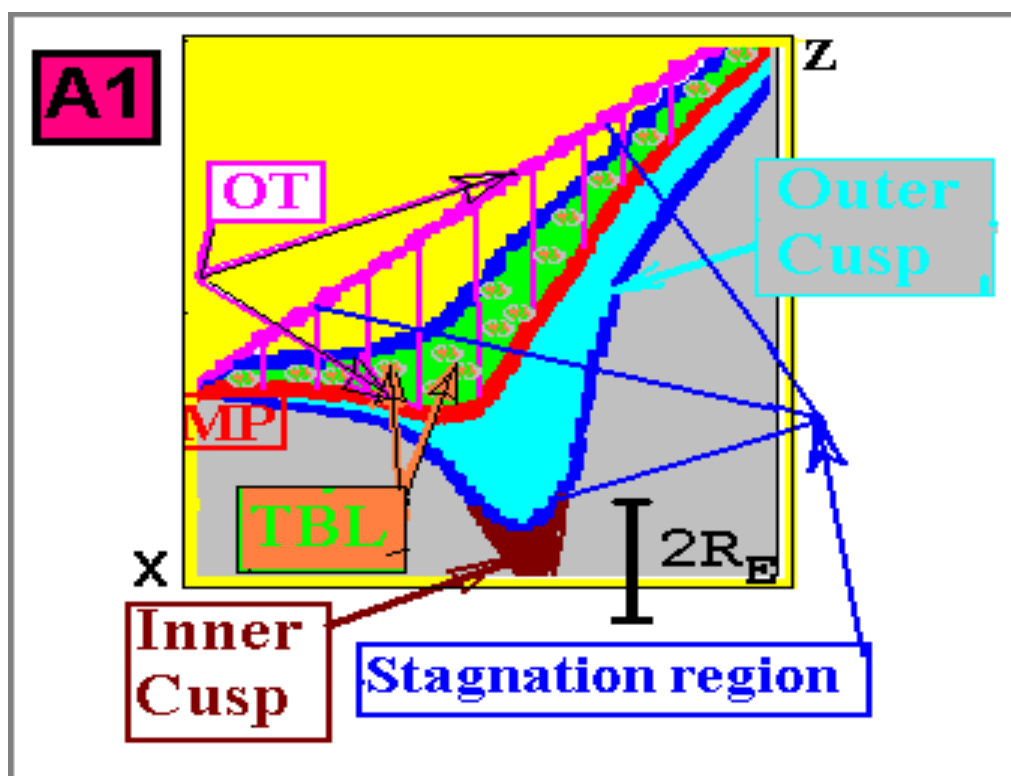


Plate A1. Characteristic regions at the magnetosheath-cusp interface for the noon meridian plane in summer period (i.e. for the positive dipole tilt): the inner and outer(OC) cusps, the outer cusp throat (OT), stagnation region, magnetopause (MP) and the turbulent boundary layer (TBL). See also the text for more details.

Plate A2 *Outbound MSH/cusp interface crossing by Interball-1 and Magion-4 on May 29, 1996. The regions depicted in Plate A1 are marked on panels a, b. Panel a: energy distribution of the protons perpendicular to the Sun-Earth line (PROMICS-3) the ion temperature T_i is depicted by black line. Panels b and c: magnetic field in the GSM coordinates. Panel d: the total energy density, E_s , black shading, the thermal energy density, $E_{thermal} = 1.5 nkT_i$ (n - plasma density, T_i - ion temperature), the kinetic energy density, $E_{kinetic} = 0.5 n M_i V_i^2$ (yellow shading, M_i and V_i - ion mass and velocity) and the magnetic energy density, $E_m = B^2/8\pi$ (dark gray shading). Panel e: GSE V_x and V_z components of ion velocity from the MHD model of Fedder et al. [1997] (black trace) and measurements by SKA-1 ion spectrometer (red colored with gray shading). Panel f: the power in the magnetic field variations, D_f , and the standard deviation of the magnetic field magnitude, D_m (in energy density units); the variations are calculated over two minute intervals with the interval shifts of 30 seconds. Panel g: Fourier spectrogram of the magnetic field power with sampling rate 4 Hz; the proton cyclotron frequency labeled 'Fcp+' is over-plotted by blue line. Panel h: magnetic spectra from Magion-4 in the range 20-2000 Hz during a period when Interball-1 observed the turbulence. Insert A shows Yamauchi and Lundin (1997) 'Laval nozzle' model sketch.*

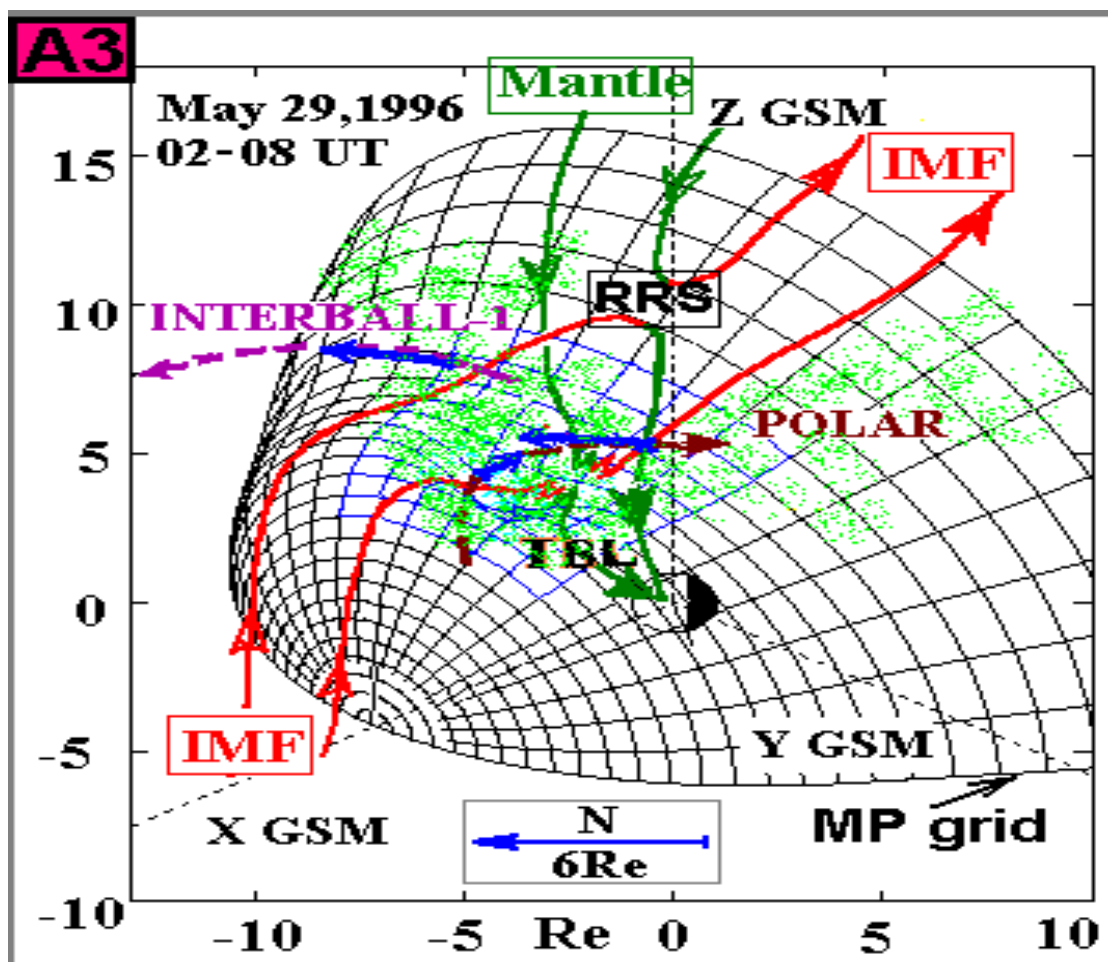


Plate A3. Sketch for reconnection at the indented magnetopause during the northward IMF conditions on May 29, 1996. Black magnetopause (MP) grid is described in section 6.2. Polar and Interball-1 orbits are shown by the dashed brown and violet lines, respectively. TBL from Figure 6 is depicted by green dots. The measured MP normals are marked by blue arrows (the total normal length is shown at the Figure bottom by blue arrow marked by 'N'). The draped IMF magnetic field lines are marked by red color, the magnetospheric/mantle lines – by green color.

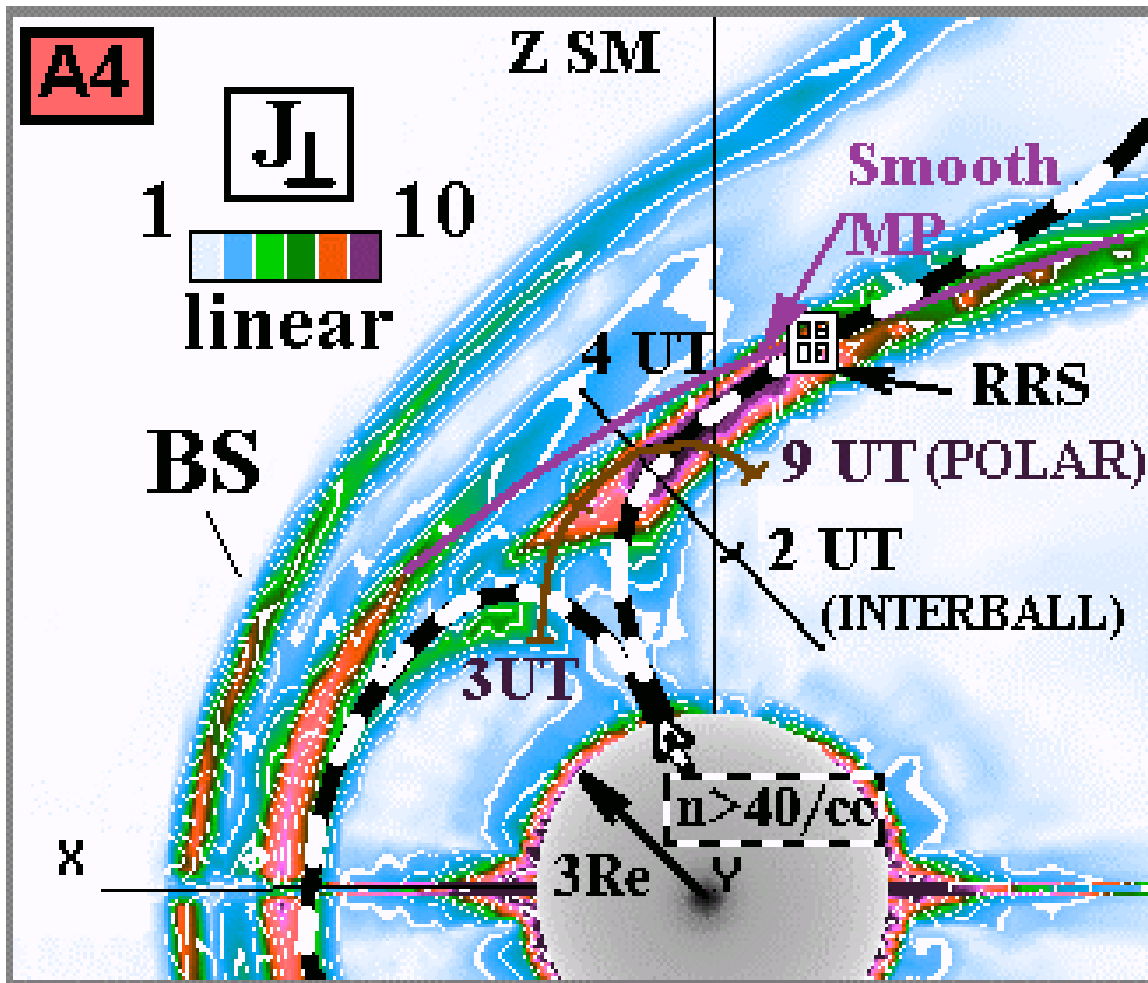


Plate A4. The distribution of the currents perpendicular to magnetic field in the noon meridian plane in SM coordinates depicted by the color scale from the global MHD model by Fedder et al., (1995). The projections of the Polar (brown trace) and Interball-1 (black trace) orbits onto that plane (Polar crossed this plane at 0530 UT) are also shown. The dayside magnetopause (MP) and bow shock (BS) are seen in the current maxima at low latitudes, the higher latitude smooth MP from Sibeck et al., (1991) model is depicted by the violet line. The global MHD model determined 'remote' (from the cusp) reconnection site (RRS) position is shown by white squared cross. The model inward boundary of the MSH plasma with density $> 40/cc$ is shown by thick black-and-white dashed line (see also Figure 5 in Russell et al., 1998).

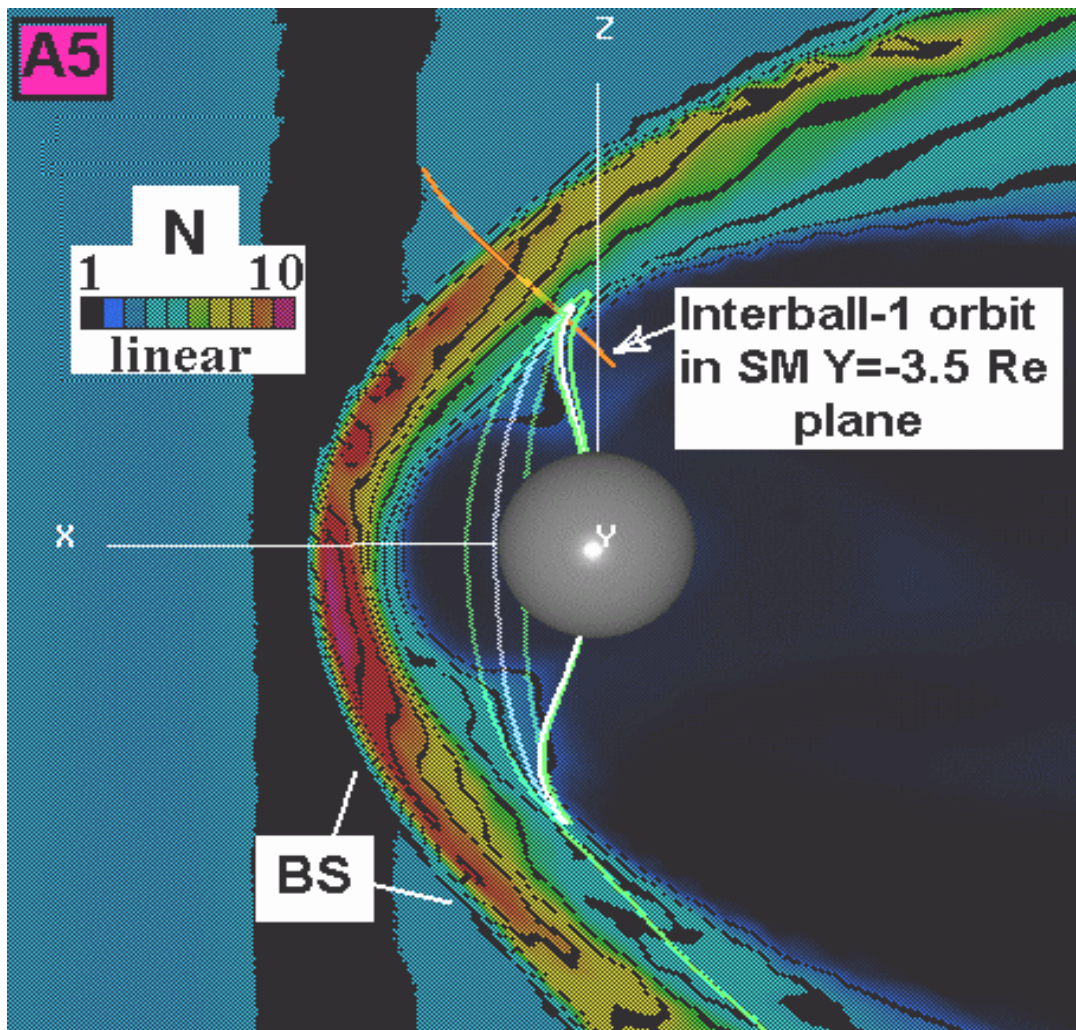


Plate A5. The plasma density from the global MHD model by Fedder et al., (1995) on the $Y=-3.5R_e$ plane and field lines through Interball orbit at 03:14 UT (white) and $\pm 0.25 R_e$ around the central field line (green). MSH corresponds the density maximum between BS and empty magnetosphere. On the closed magnetospheric lines (white and inner green ones) density enhancements are seen sunward these kinked lines (which are mostly out of the semi-transparent density plane). The outer from the Earth green field line is the reconnected one.

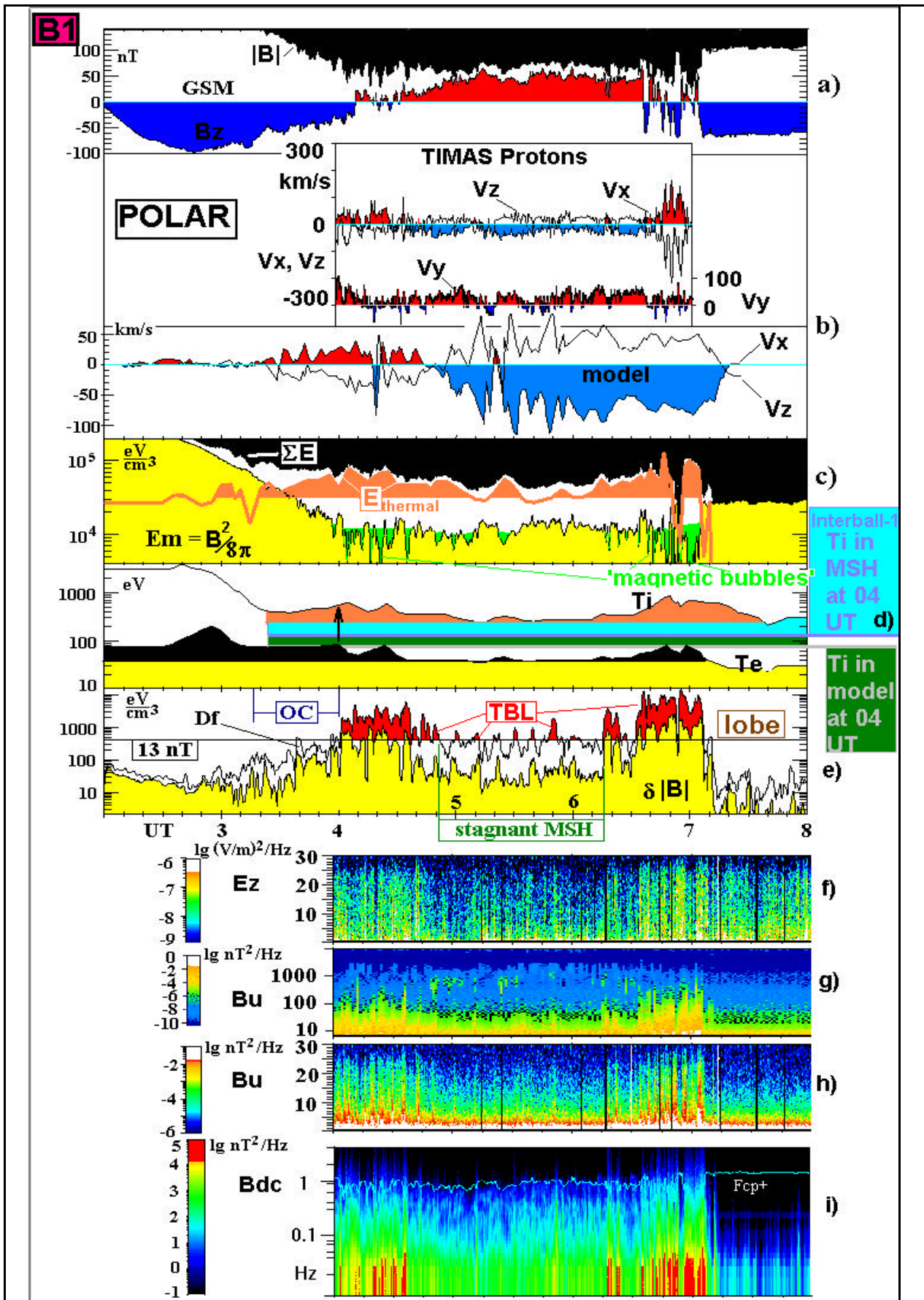


Plate B1 Particle and field parameters on Polar on May 29, 1996. Panel a: the magnetic field $|\mathbf{B}|$ (black shading) and GSM B_z (blue/ red shading for the negative and positive values). Panel b: GSM V_x and V_z components of ion velocity from the global MHD model (Fedder et al., 1997) and vector velocities of protons by TIMAS spectrometer, V_x and V_y are red/ blue shadowed for positive/ negative values. Panel c: the total energy density, E_s , (black shading), the thermal energy density (brown shading above the minimum value in MSH/ TBL), and the magnetic energy density (yellow shading). Panel d: the average ion energy T_i (the difference between the minimum T_i from Polar and the characteristic T_i in MSH from Interball-1 at 04 UT is blue-shadowed; the difference between the T_i in MSH and T_i in MSH from the MHD model at 04 UT is green-shadowed) and average electron energy T_e (yellow shading, T_e above minimum in MSH/ TBL is black-shadowed) from HYDRA. Panel e: the magnetic field variations calculated in the same way as on panel f of Plate A2; the TBL is red-shadowed, the characteristic regions marked according Plate A1. Panels f, g and h: electric E_z and magnetic (B_u) Fourier spectrograms in the spacecraft frame from PWI instrument (note the linear frequency scale on the vertical axes for E_z and low frequency B_u (panel h) and the logarithmic scale on panel g). Panel i: Fourier spectrogram of the total power of DC magnetic field (sampling rate 8 Hz, MFE experiment); the blue line depicts the proton cyclotron frequency labeled F_{cp+} .

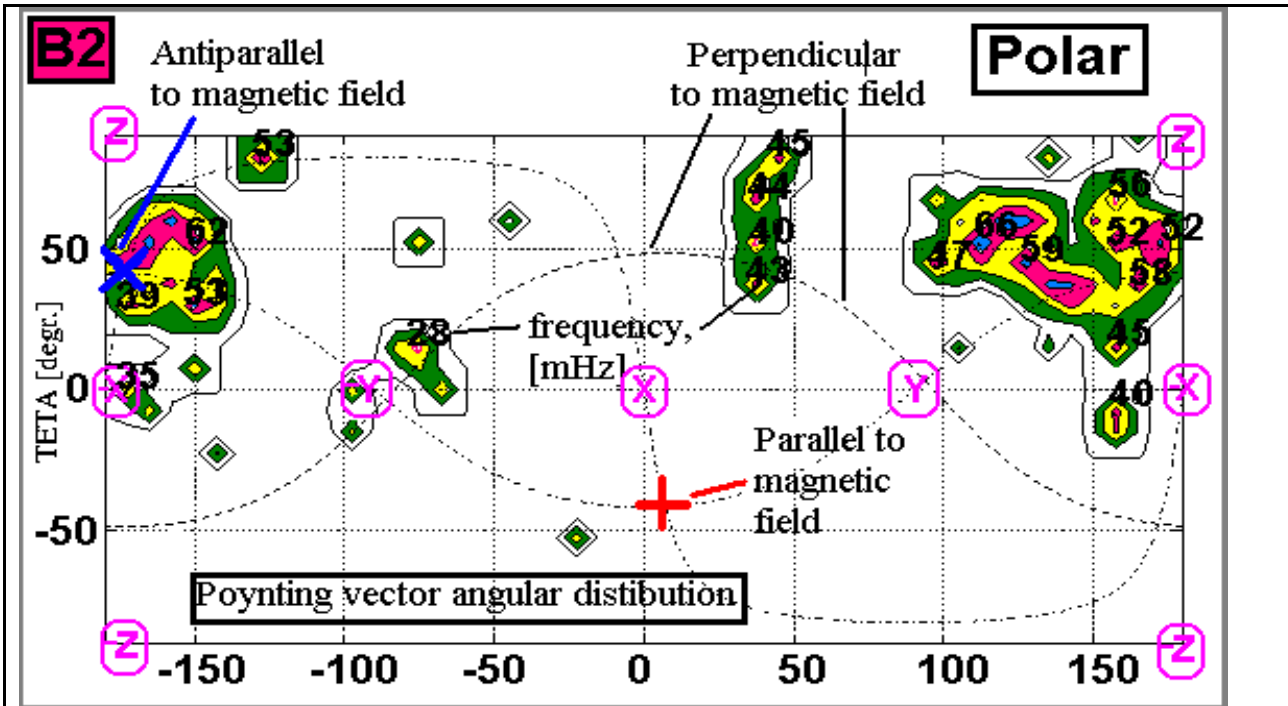


Plate B2. 07:00:00-07:01:56 UT: angular distribution of the Poynting flux in GSM from Polar; median frequency of the maxima are given in mHz;

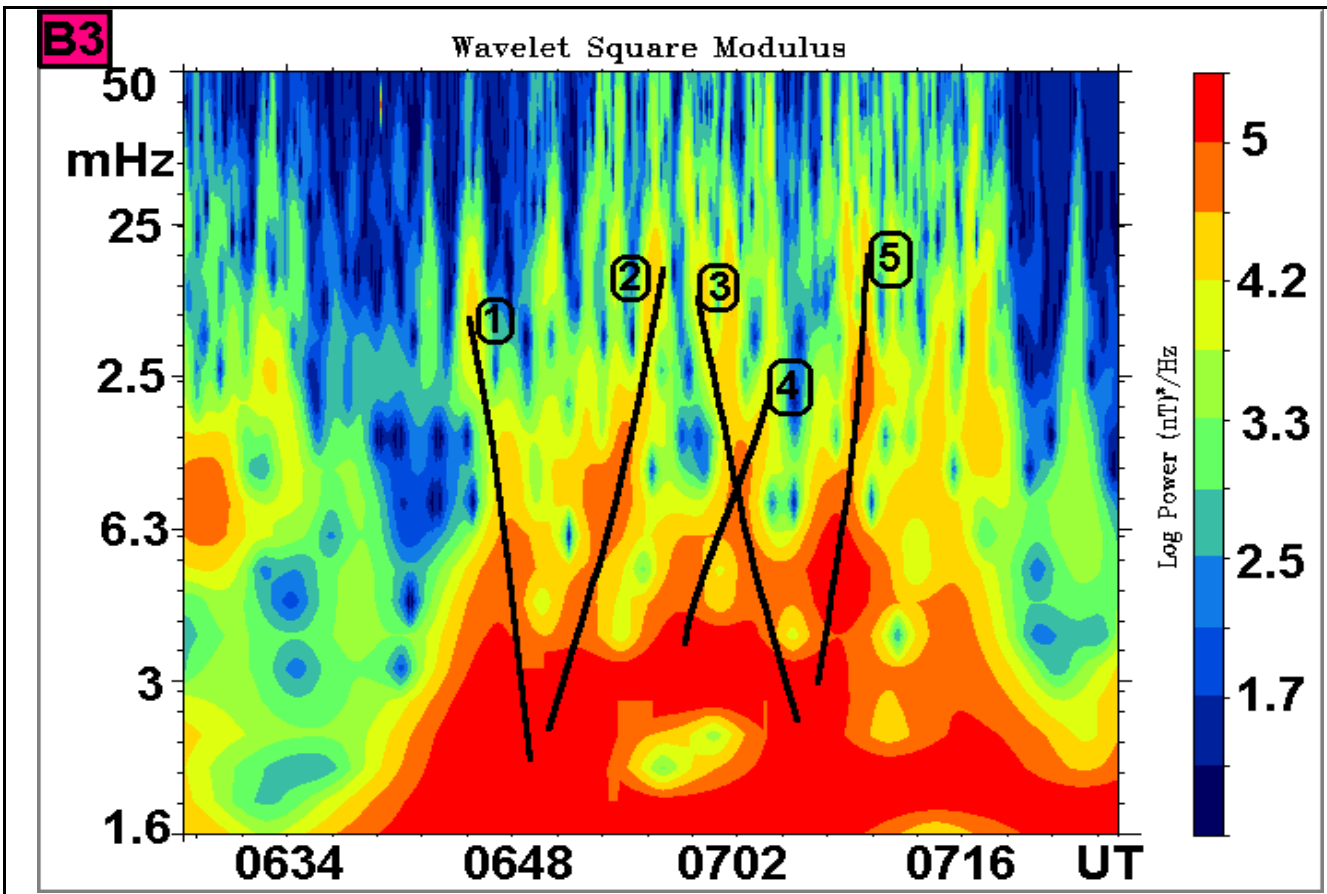


Plate B3 Wavelet spectrogram (B_z SM): Polar TBL (see Plate B1), numbered black lines mark the inferred wave cascades (2, 4, 5 – direct cascades, 1, 3 – inverse cascades, see text for further details).

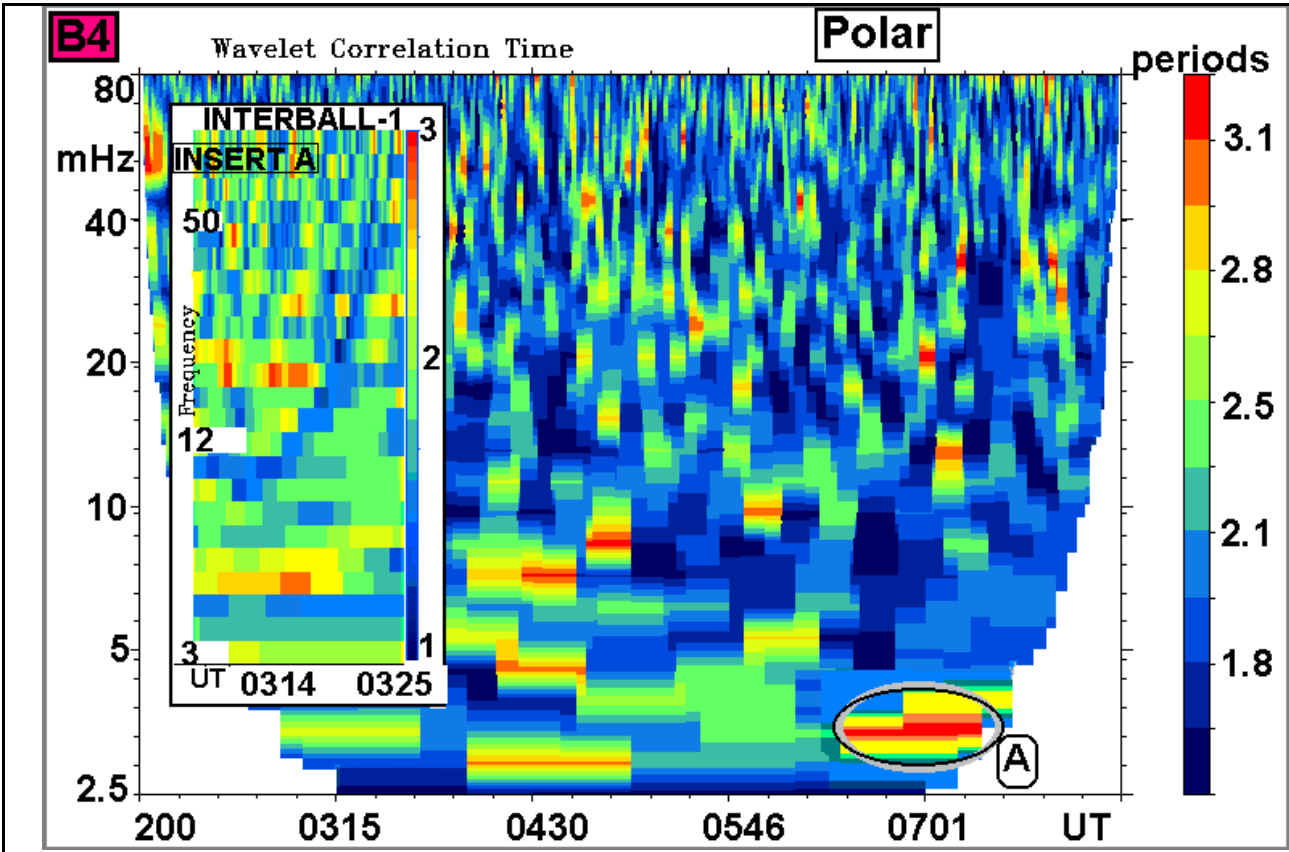


Plate B4 Wavelet correlation time for SM Bz from Polar in the TBL (see Plates B1 and B3). Label 'A' stands for the coherent structure depicted in Plate B3. Insert A: the same for Interball-1 GSM By (see text for further details).

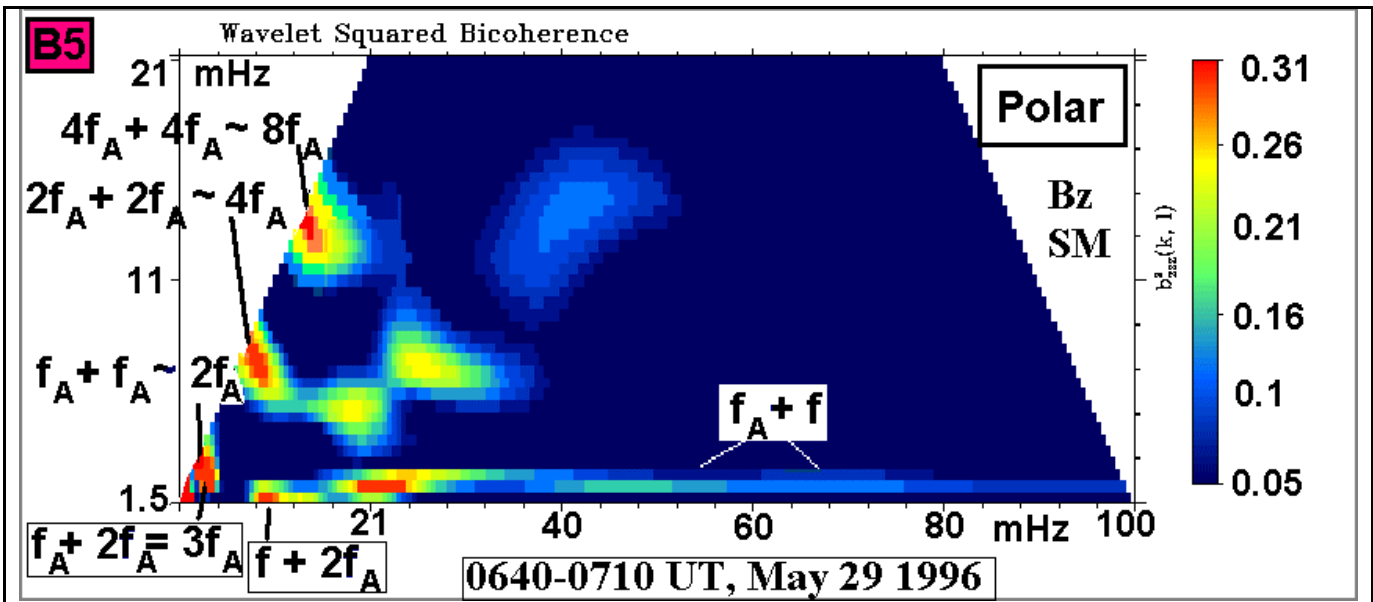


Plate B5 Wavelet bi-spectra from Polar for SM Bz in the inbound TBL at 0640-0710 UT on May 29, 1996 (cf. Plate B3 and Plate B4); the frequency f_A corresponds to that labeled 'A' in Plate B4. $f_A + f_A = 2f_A$ etc. corresponds to the harmonic generation (see also text).

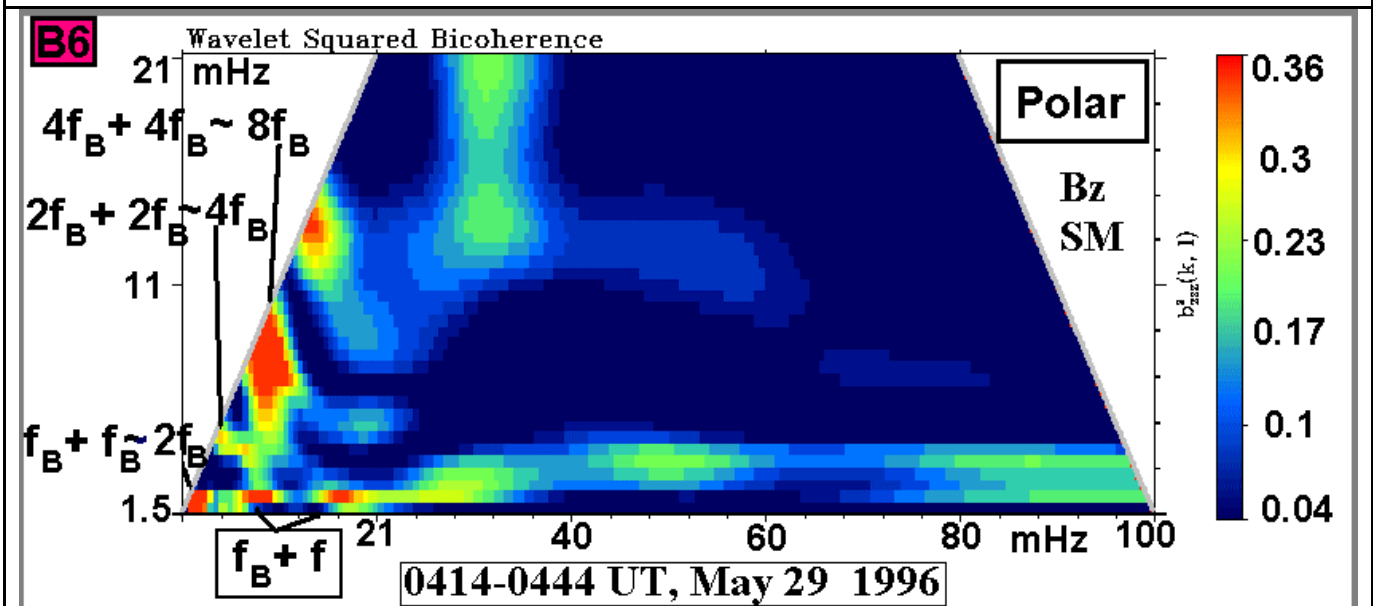


Plate B6. The same as for Plate B5 for Polar outbound TBL at 0414-0444 on May 29, 1996 (cf. Plate B3 and Plate B4).

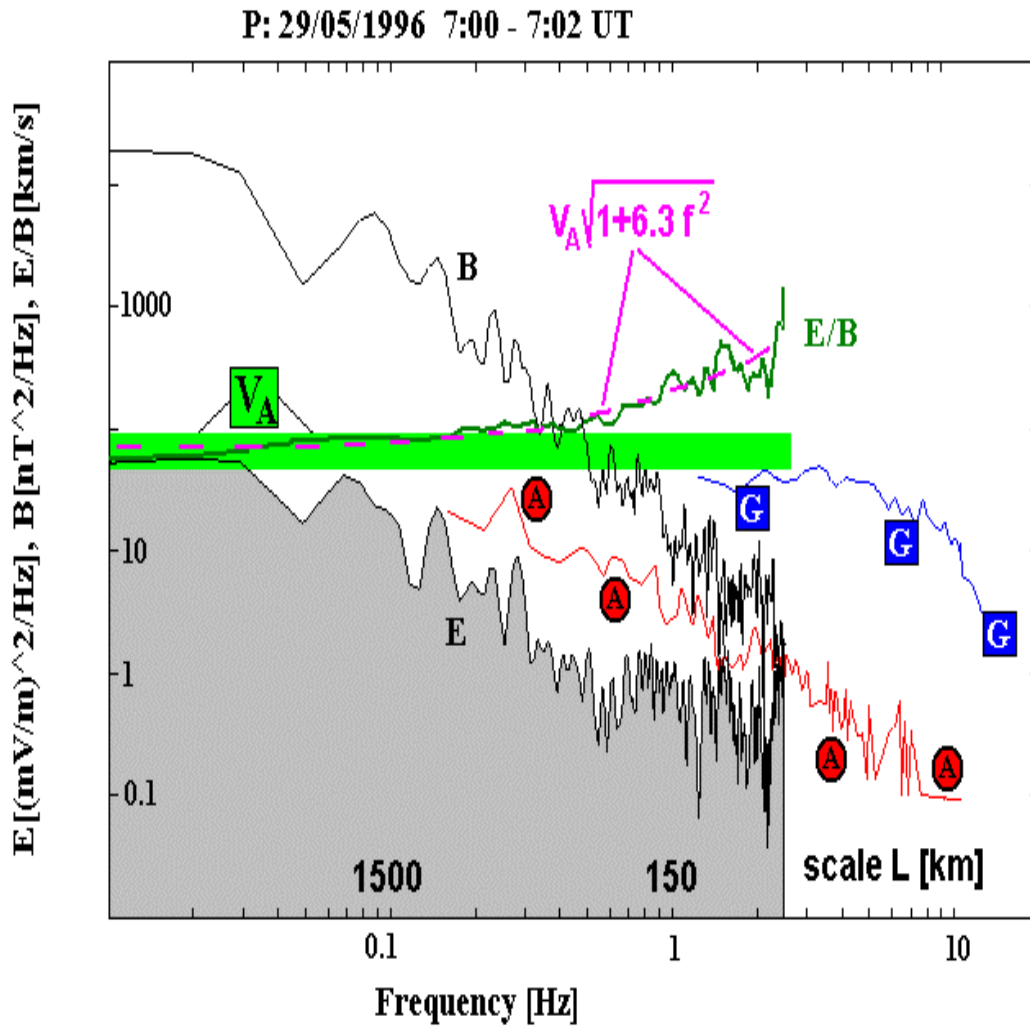


Fig. 1A. Electric (E, gray shadowed) and magnetic (B) Fourier spectra from Polar at 0700-0702 UT on May 29, 1996, E/B – thin green line (in km/s); dashed line- KAW frequency dependence for E/B from equation (1); Alfvén speed V_A - thick green line. Squared 'G': Geotail electric spectra in TBL, 11:38- 11:42 UT, August 27, 1995. Circled 'A': electric spectrum in cusp, Interball-2, 0058 UT, Jan. 22, 1997.

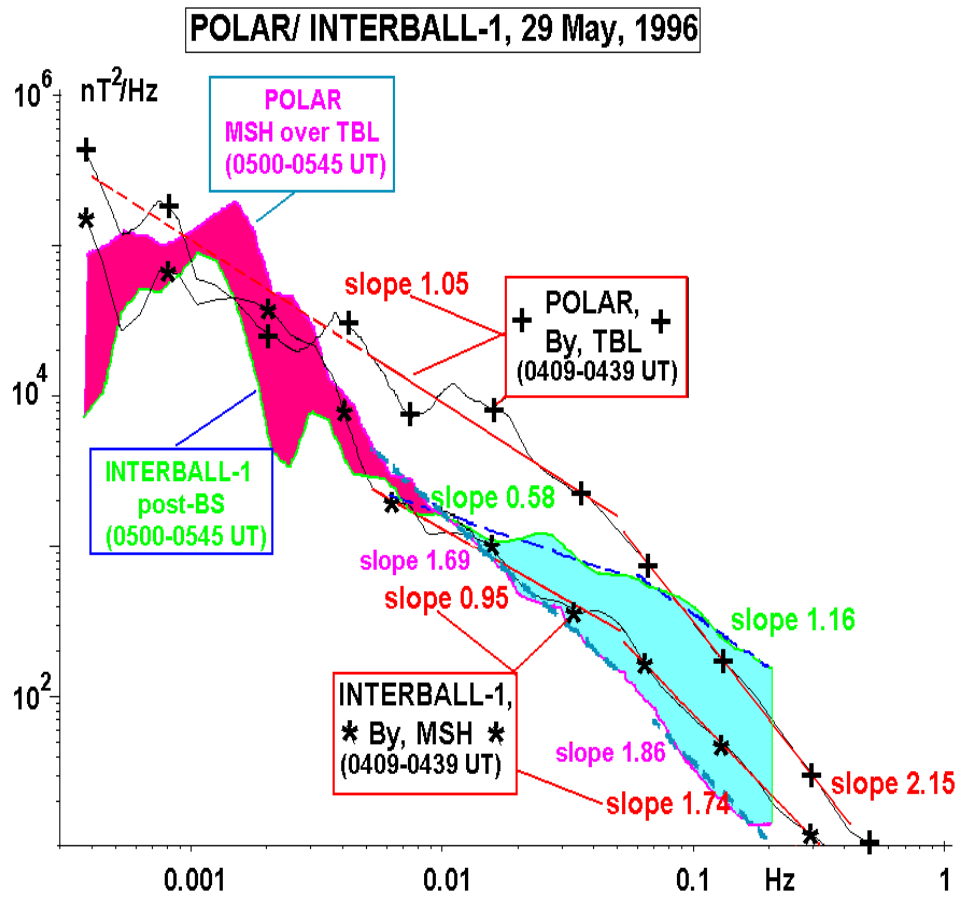


Fig. 1B. Magnetic wavelet spectra of GSM B_y on May 29, 1996. Polar: TBL at 04:09-04:39 UT (crosses, the characteristic slopes are marked by the red color) and stagnant MSH over TBL at 05:00-05:45 UT (violet trace, the difference with the simultaneous post-BS spectrum from Interball-1 is shadowed). Interball-1: MSH at 04:09-04:39 UT (asterisks, the characteristic slopes are marked by the red color) and post bow shock MSH at 05:00-05:45 UT (green trace).

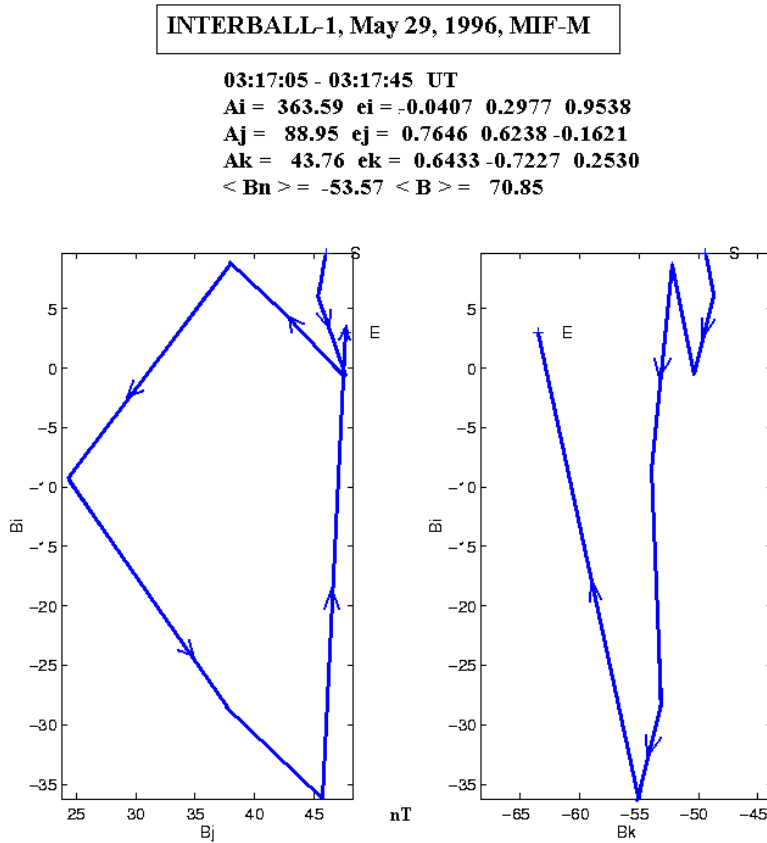


Fig. 2A. Magnetic field hodogram of the Interball vortex-like structure in the main MP current sheet on May 29, 1996. The vortex scale in the minimum variance direction is estimated by ~ 1000 km (see text for details). The maximum, medium and minimum variance eigen values and eigen vectors are given at the Figure top in the GSM coordinate system along with the average normal component $\langle B_n \rangle$ and the magnetic field magnitude $\langle B \rangle$.

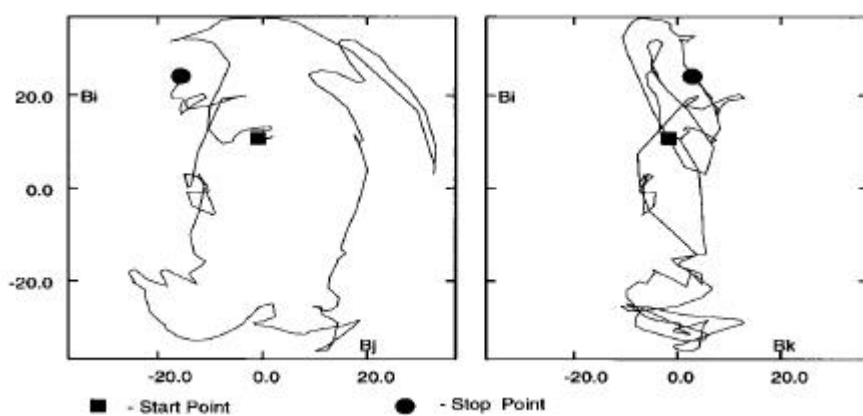


Fig. 2B. Magnetic field hodogram of the Polar vortex-like structure in the main MP current sheet on May 29, 1996 at 070043- 070052 UT. The maximum, medium and minimum variance eigen values and eigen vectors in the SM coordinate system are: $A_i = 505.9$, $e_i = (0.39; -0.46; 0.8)$; $A_j = 204.4$, $e_j = (0.14; -0.83; -0.55)$; $A_k = 28$, $e_k = (0.91; 0.33; -0.26)$.

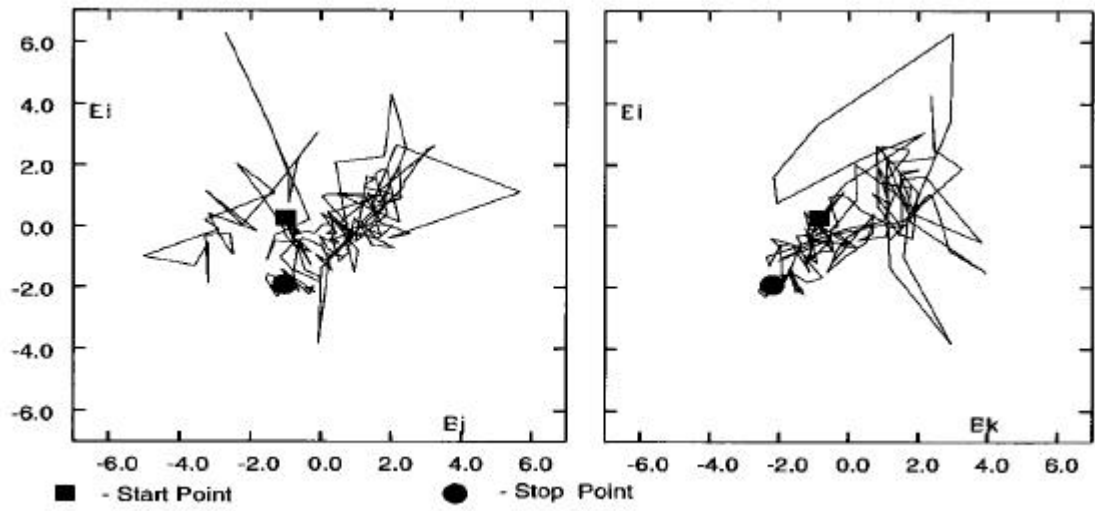


Fig. 2C. Electric field hodogram of the Polar vortex-like structure on May 29, 1996 (see Figure 2B) in the same coordinate system as Figure 2B.

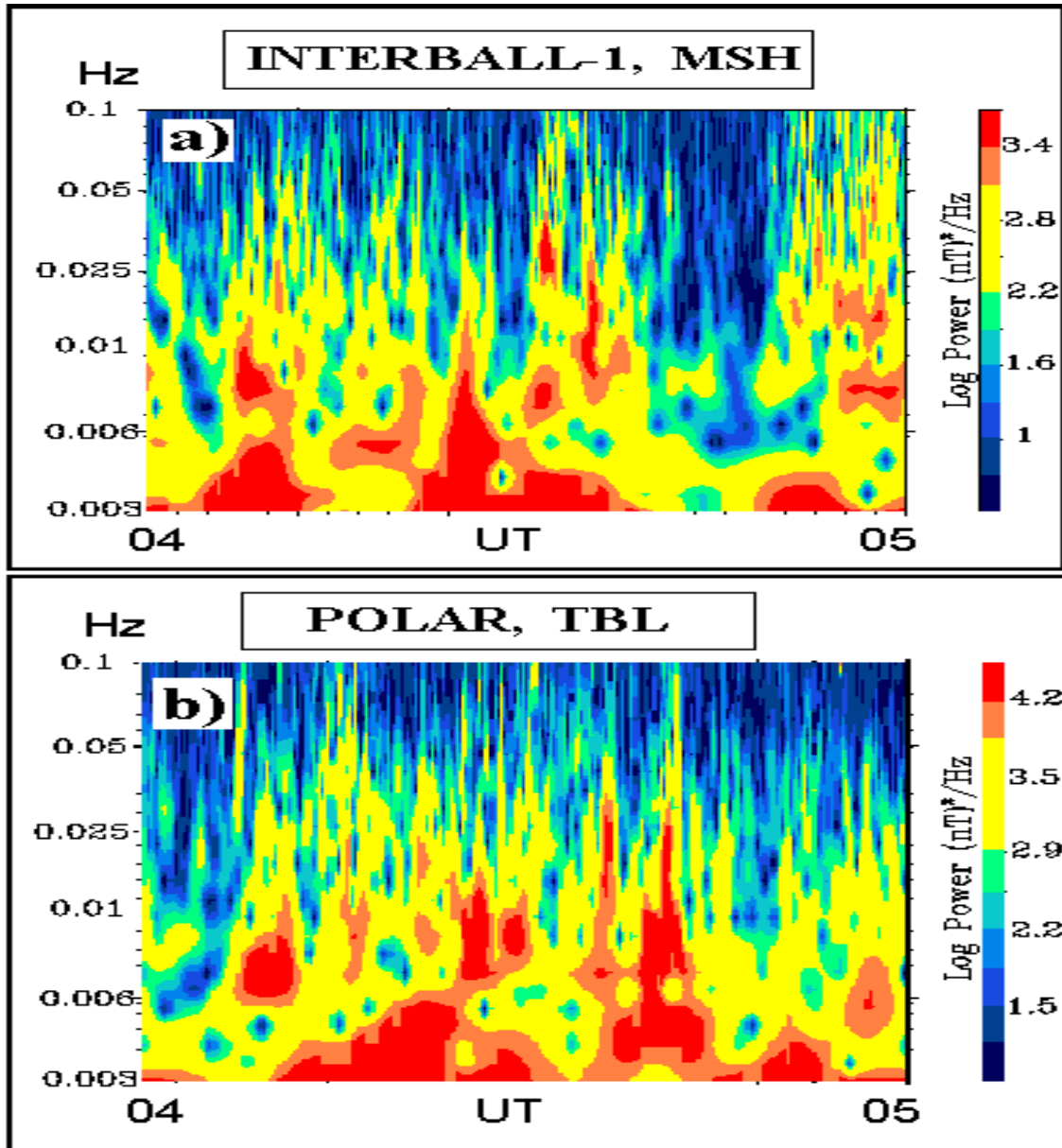


Fig. 3. (a) Interball-1 wavelet spectrogram in MSH (By GSM component, 0.003- 0.1 Hz) at 04- 05 UT (see also Plate A1);

(b) the same for Polar in TBL (see also Plate B1).

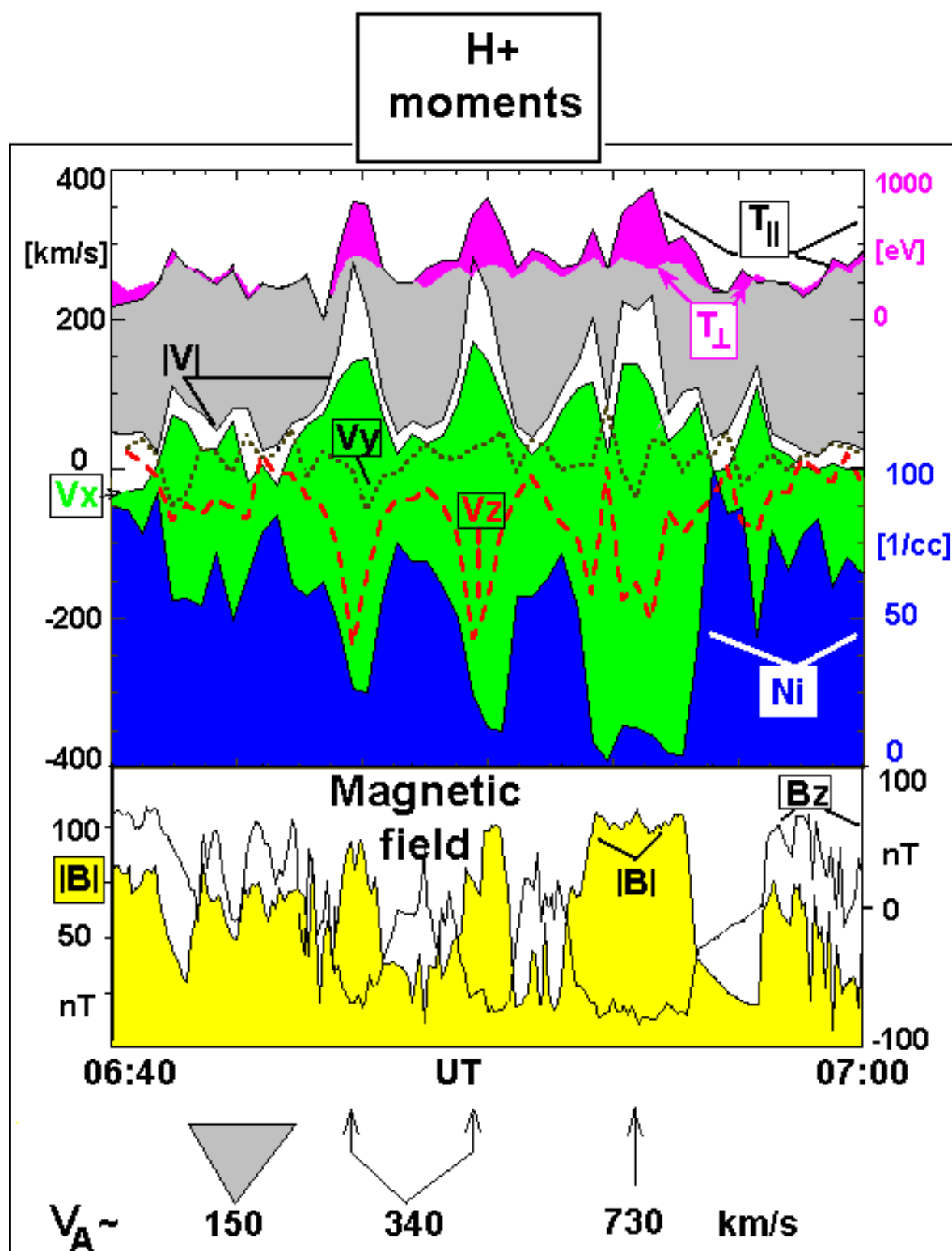


Fig 4. Coherent structure in the inbound TBL from Polar (see Plates B1, B3, B5). Top panel: TIMAS proton moments temperature (violet shading depicts the difference between the parallel and perpendicular temperatures), velocity (V_x - green shading, V_y - dots, V_z - red dashed line) and density (blue shading). Bottom panel: magnetic field B_z (the scale at the right) and $|B|$ (yellow shading, the scale at the left). Bottom line: Alfvén velocity in MSH (gray triangle) and inside high-speed jets (arrows).

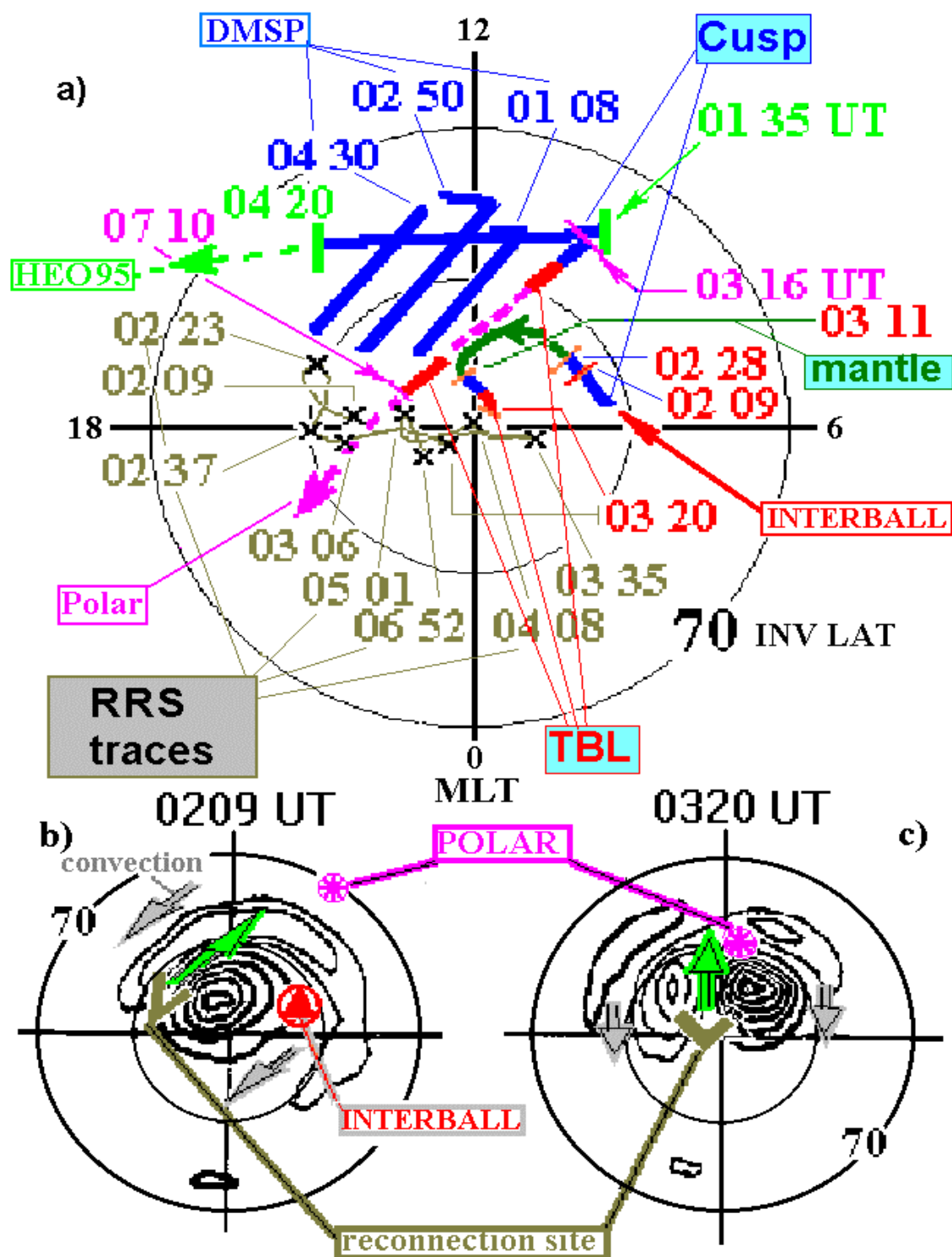


Fig. 5. Projection onto northern ionosphere in (Invariant Latitude/ MLT) coordinates on May 29, 1996. (a) Cusp (blue), mantle (green), TBL (red) ionospheric traces for different UT and spacecraft, marked in the Figure and the traces of remote reconnection sites (RRS) for different UT from the global MHD model (inclined crosses) (b) ionospheric equipotential contours for cross-cap potential 6 kV and field-aligned current 4×10^{-6} A/m. at 0209 UT from the global MHD model and (c) the same for 0320 UT. Traces of Polar (violet asterisks), Interball-1 (red circled triangle) and reconnection point footprints (RRS, brown arrows) are depicted along with the convection directions (along the contours, green arrows in the center and gray ones at the periphery).

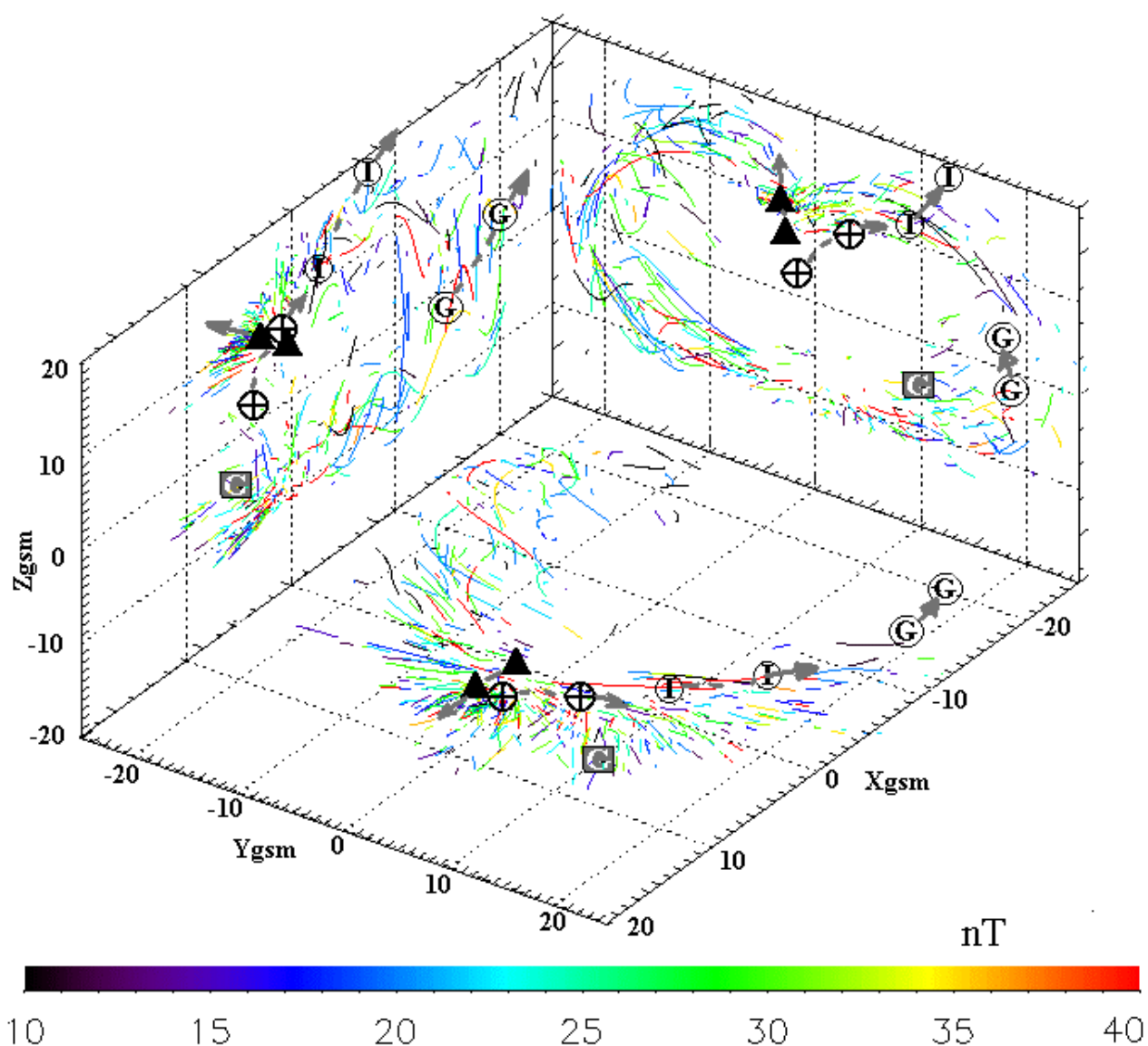


Fig.6. TBL in 1995 - 1998 from Interball-1 magnetic field data. The full standard deviation is color-coded according to the scale at the Figure bottom. Case studies are shown by symbols (circled crosses and triangles – for Polar and Interball-1 on May 29, 1996, for the rest symbols see text)